Summer 8-22-2021

ANALYZING NANOSCALE THERMAL TRANSPORT USING TIME-RESOLVED X-RAY DIFFRACTION

James Grammich
DePaul University, JGRAMMIC@depaul.edu

ANALYZING NANOSCALE THERMAL TRANSPORT USING TIME-RESOLVED X-RAY DIFFRACTION

A Thesis

Presented in

Partial Fulfillment of the

Requirements for the Degree of

MASTER OF SCIENCE

2 0 2 1

BY

James Grammich

PHYSICS DEPARTMENT

College of Science and Health

DePaul University

Chicago, Illinois

ACKNOWLEDGEMENTS

I would like to thank Dr. Eric Landahl for being my advisor during my time here at DePaul. In addition to helping me with this project, Dr. Landahl has helped me to become a better scientist. Additionally, I would also like to thank Dr. Bernhard Beck-Winchatz and Dr. Gabriela Gonzalez Aviles for serving on my thesis committee.

The initial version of the *TRXD* code was written by former DePaul Physics graduate student Dr. G. Jackson Williams (now at Lawrence Livermore National Laboratory), and further developed by Dr. Landahl. Initial tests of the code were conducted by DePaul Physics undergraduate students Danielle Leppert-Simenauer and Sinead Humphrey. Data analyzed in this experiment was taken by DePaul Physics undergraduate students Grace Longbons and Timothy Holmes, along with Dr. Landahl, Dr. Don Walko (Argonne National Laboratory), Dr. WonHyuk Jo (now at DESY), and Dr. Sooheyong Lee (KRISS). Samples were provided by KRISS.

Benchmarking of TRXD in this study was performed using program *GID_SL* at Sergey Stepanov's X-Ray Server, `https://x-server.gmca.aps.anl.gov` .

Use of the Advanced Photon Source was supported by the U.S. Department of Energy, Basic Energy Sciences, Office of Science, under Contract No. DE-AC02-06CH11357.

I would like to thank everyone at the DePaul Physics department. You have all helped me grow tremendously, and made my time here immensely enjoyable.

Lastly, I want to thank all of my family and friends outside of DePaul who have provided me with support and encouragement these past few years.

TABLE OF CONTENTS

LIST OF FIGURES

LIST OF FIGURES – *Continued*

LIST OF FIGURES – *Continued*

LIST OF FIGURES – *Continued*

LIST OF FIGURES – *Continued*

LIST OF TABLES

ABSTRACT

Classical models of thermal transport breakdown at lengthscales below a few microns in many materials, including the surfaces of bulk semiconductors. This presents difficulties in the analysis and design of small electronic devices, where unexpected thermal effects can occur such as hot spots that deteriorate performance and limit speed. Time-resolved x-ray diffraction has been proposed as one method to investigate this regime of nanoscale thermal transport, especially inside semiconductor materials where other techniques can not penetrate or yield quantitative results. Towards this goal, this thesis benchmarks a new, portable, and fast open-source x-ray dynamical diffraction code (*TRXD*) for strained crystals developed by DePaul University against an existing standard server-based closed-source calculation tool (*GID_SL*, Grazing Incidence Diffraction for Superlattices). *TRXD* is also validated against experimental x-ray peak lineshapes by convolving the calculation results with an appropriate instrumentation resolution function. *TRXD* is shown to properly predict the long time-scale classical thermal behavior of a cooling semiconductor, while revealing discrepancies at the short time-scale where new nanoscale thermal transport models are under development. A new high-resolution x-ray diffraction data set is compared to a previously published low-resolution data set, and found to give the same result for delayed thermal transport in ultrafast laser-excited 100 nm metal film on a Gallium Arsenide crystal substrate.

CHAPTER 1

Introduction

1.1 Thesis motivation

The Fourier Law of Heat Conduction describes heat transfer at macroscopic length scales (generally over 10 microns at room temperature). The Law states that heat flow is proportional to the negative gradient of temperature [1] and can be expressed mathematically as a diffusion equation,

$$\frac{\partial T}{\partial t} = \alpha \nabla^2 T \tag{1.1}$$

where T is temperature, t is time, and α is a constant termed the *thermal diffusivity*. Recently, it has become well known that this textbook partial differential equation breaks down at length scales comparable to or shorter than the phonon Mean Free Path (MFP), where ballistic transport may significantly alter thermal conductivities in semiconductors and insulators [2]. This is the signature phenomenon of "nanoscale thermal transport" [3] : electronic devices built for small size and high speed may develop unanticipated hot spots resulting in reduced performance and lifetime [4]. These implications are particularly significant for next generation Light Emitting Diodes, thermoelectric devices for waste heat recovery, photovoltaics, optoelectronics, and high speed integrated circuits [5].

To date, almost all experimental studies of phonon MFP are based upon one of two indirect measurement techniques: ultrafast optical methods and Inelastic Neutron Scattering (INS). Most recent and prominent are measurements of surface temperature using optical techniques [6]. In these methods, the surface temperature of a bulk material or heterostructure is monitored following spatial [7] or temporal [8]

modulation of surface heating (usually with a short-pulse later). The bulk behavior is then inferred from the surface temperature evolution. The time-dependent surface temperature has been found to change depending upon modulation frequency; the thermal conductivity value is seen to increase monotonically as the modulation wavelength increases past the phonon mean free path. This "accumulation" method of phonon MFP spectroscopy has yielded several insights. For instance, low-frequency phonons carry thermal energy very long distances, but rely on scattering with high-frequency phonons to locally equilibrate [9]. Thus, details of the phonon density of states (DOS) may have significant impact on the phonon lifetime, and thereby the MFP and conductivity. This has brought about a renewed interest in INS for phonon dispersion and lifetime measurements [10].

There are several limitations implicit in these methods. First, the optical techniques only allow surface temperature to be measured. Deviations from the depth-dependent temperature profile are presumed, but have not been verified. Second, the exploration of transport across defects has been extremely limited, since the accumulation techniques are not very sensitive to sub-surface modifications which affect mostly high-frequency phonons which cannot be clearly isolated from the "accumulated" spectra. Third, the major technological issue associated with nanoscale thermal transport are buried interfaces, which are all but invisible to optical techniques. In 2007, a research team including Prof. David Cahill (UIUC) and Dr. Eric Landahl (now at DePaul University) participated in an early attempt to observe ballistic transport using Time-Resolved X-Ray Diffraction (TRXD) at APS 7ID [11]. Their approach was to construct a depth-dependent temperature probe by burying layers at different depths within metal-coated semiconductor samples. The buried layers acted as thermometers at different locations, and using kinematical diffraction they were able to show a significant discrepancy in both heat transit time and maximum temperature between the Fourier Law and the buried layer data, and proposed that a multi-channel model of phonon conductivity was needed. A related paper [12] showed it was possible to use TRXD to watch thermal transport

across a buried interface and measure the thermal (or "Kapitza") resistance.

X-ray techniques have made no significant contribution to nanoscale thermal transport since this time. However, recent improvements in TRXD techniques [13] and detectors [14] present the possibility of employing sophisticated analysis [15, 16, 17] to reliably reconstruct transient 3D stress profiles beneath the surface of a laser-excited semiconductor [18]. Based on these advances, a recent experimental effort was led by DePaul University to measure temperature as a function of depth and position (i.e., $T(t, z)$) using TRXD to directly validate transport models, with the ultimate experimental goal to extract the phonon MFP spectra directly. **This thesis presents the initial analysis of this dataset.**

1.2 Classical theory of heat transport

1.2.1 Overview

The specific problem considered here is the one-dimensional calculation of heat transport from an ultrafast (sub-picosecond) laser excited metal film into a substrate, as illustrated in Fig. 1.1. This problem is considered both because it is experimentally realizable, and also because it is an idealized abstraction to many situations found inside compact electronic devices in which metal electrodes layered onto crystalline semiconductors are rapidly heated by fast switching currents (e.g. Field Effect Transistors). First, the incident laser rapidly ($\approx$ 1 ps) raises the temperature of the film uniformly because metal has many free electrons to distribute energy quickly. The film has been deposited on top of a bulk material, which is initially at a uniform colder temperature near room temperature. The specific experiment that is considered here is a 100 nm thick chromium film sputtered on top of a bulk crystalline Gallium Arsenide wafer. The wafer is 500 μm thick, has a (100) surface orientation, and an area of approximately 1 cm^2.

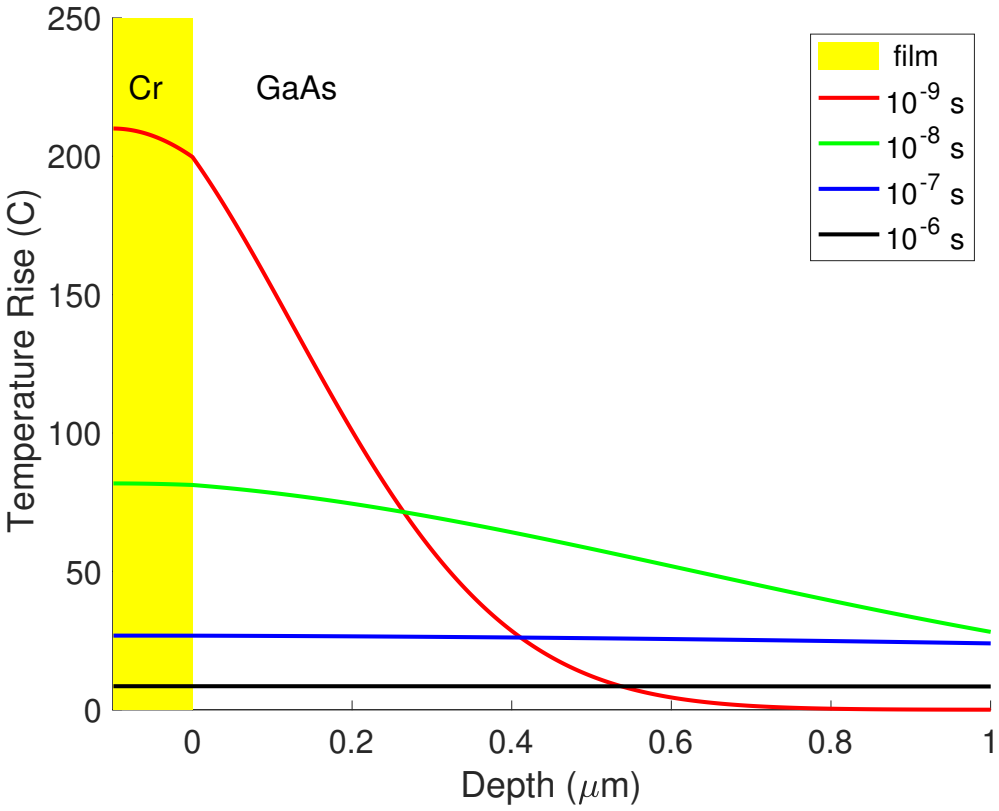

Figure 1.1: Results of the classical thermal transport equation as described here, applied to a 100 nm thick Cr film on a bulk GaAs substrate following heating by an ultrafast laser pulse of 14.8 mJ/cm^2. This matches the experimental conditions studied in this thesis. The thermal profile is smooth across the interface, but has a discontinuity in the first derivative due to the different thermal properties of the film and substrate. The temperature profile flattens as time increases after the initial rapid heating. The x-ray probe depth is approximately the micron depth displayed in the figure, although simulations are run out to 10 μm.

1.2.2 Solving the diffusion equation

These results are taken from Example 10.8 of Hahn and Ozisik, *Heat Conduction* [19]. They consider a one-dimensional, two-layer composite slab with a film of thickness L on top of a semi-infinite bulk material; this problem is illustrated in Fig. 1.1. The layers are presumed to be in perfect thermal contact with the film region initially at a uniform temperature T_0 (caused by rapid laser energy absorption) and bulk region at zero temperature. The problem is easiest stated using a dimensionless temperature $\theta_i(x,t)$ defined as as

$$\theta_i(x,t) = \frac{T_i(x,t)}{T_0}, \quad i = film, bulk \tag{1.2}$$

with T_i referring to the temperature of the film or bulk, T_0 referring to the initial temperature, x is referring to depth, and t is referring to time. We can formulate the problem of the change in temperature past time 0 (when the laser strikes the sample) as

$$\frac{\partial^2 \theta_{film}}{\partial x^2} = \frac{1}{\alpha_{film}} \frac{\partial \theta_{film}(x,t)}{\partial t} \quad 0 < x < L \tag{1.3}$$

and

$$\frac{\partial^2 \theta_{bulk}}{\partial x^2} = \frac{1}{\alpha_{bulk}} \frac{\partial \theta_{bulk}(x,t)}{\partial t} \quad L < x \tag{1.4}$$

where α_{film} and α_{bulk} are the thermal diffusivity constants associated with the film and bulk respectively, and L is the point where the film and bulk meet. The boundary conditions for this problem are

$$\left.\frac{\partial \theta_{film}}{\partial x}\right|_{x=0} = 0 \tag{1.5}$$

$$\theta_{film}(L,t) = \theta_{bulk}(L,t) \tag{1.6}$$

$$k_{film} \left.\frac{\partial \theta_{film}}{\partial x}\right|_{x=L} = k_{bulk} \left.\frac{\partial \theta_{bulk}}{\partial x}\right|_{x=L} \tag{1.7}$$

$$\theta_{bulk}(x \to \infty, t) \to 0 \tag{1.8}$$

where $k_{film,bulk}$ are the thermal conductivities. The conditions of the film and bulk at time 0 are

$$\theta_{film}(x,0) = 1 \quad 0 < x < L \tag{1.9}$$

$$\theta_{bulk}(x,0) = 0 \quad L < x \tag{1.10}$$

At this point, the Laplace transformation is applied both to the model equations and boundary conditions, to generate ordinary differential equations that can be solved for the changes in temperature. The resulting equations and boundary conditions are

$$\frac{d^2\bar{\theta}_{film}(x,s)}{dx^2} = \frac{1}{\alpha_{film}}[s\bar{\theta}_{film}(x,s) - 1] \tag{1.11}$$

$$\frac{d^2\bar{\theta}_{bulk}(x,s)}{dx^2} = \frac{1}{\alpha_{bulk}}s\bar{\theta}_{bulk}(x,s) \tag{1.12}$$

$$\frac{d\bar{\theta}_{film}}{dx}\Big|_{x=0} = 0 \tag{1.13}$$

$$\bar{\theta}_{film}(L) = \bar{\theta}_{bulk}(L) \tag{1.14}$$

$$k_{film}\frac{d\bar{\theta}_{film}}{dx}\Big|_{x=L} = k_{bulk}\frac{d\bar{\theta}_{bulk}}{dx}\Big|_{x=L} \tag{1.15}$$

$$\bar{\theta}_{bulk}(x \to \infty) \to 0 \tag{1.16}$$

where $\bar{\theta}_i$ is the Laplace transform of the normalized temperature θ and s is the Laplace transform of the depth position x. Applying the boundary functions these resulting equations, the solutions for these ODEs are

$$\bar{\theta}_{film}(x,s) = \frac{1}{s} - \frac{1-\gamma}{2s}\frac{e^{-\sigma(L-x)} + e^{-\sigma(L+x)}}{1-\gamma e^{-2\sigma L}} \quad 0 \le x < L \tag{1.17}$$

$$\bar{\theta}_{bulk}(x,s) = \frac{1+\gamma}{2s}\frac{e^{-\sigma\mu(x-L)} - e^{-\sigma(2L+\mu x-\mu L)}}{1-\gamma e^{-2\sigma L}} \quad L < x \tag{1.18}$$

where

$$\sigma \equiv \sqrt{\frac{s}{\alpha_{film}}} \tag{1.19}$$

$$\gamma \equiv \frac{\beta - 1}{\beta + 1} \tag{1.20}$$

$$\beta \equiv \frac{k_{film}}{k_{bulk}}\mu. \tag{1.21}$$

$$\mu = \sqrt{\frac{\alpha_{film}}{\alpha_{bulk}}} \tag{1.22}$$

The inverse Laplace transform pairs,

$\bar{F}(s)$	$F(x)$
$\frac{1}{s}$	1
$\frac{1}{s}e^{-k\sqrt{x}} \quad k \geq 0$	$erfc(\frac{k}{2\sqrt{x}})$

can now be applied to find the classical model for the temperature profiles,

$$\theta_{film}(x,t) \equiv 1 - \frac{1-\gamma}{2}\sum_{n=0}^{\infty}\gamma^n\left\{erfc\left[\frac{(2n+1)L-x}{2\sqrt{\alpha_{film}t}}\right] + erfc\left[\frac{(2n+1)L+x}{2\sqrt{\alpha_{film}t}}\right]\right\} \quad 0 < x < L \tag{1.23}$$

$$\theta_{bulk}(x,t) \equiv \frac{1+\gamma}{2}\sum_{n=0}^{\infty}\gamma^n\left\{erfc\left[\frac{2nL+\mu(x-L)}{2\sqrt{\alpha_{film}t}}\right] - erfc\left[\frac{(2n+2)L+\mu(x-L)}{2\sqrt{\alpha_{film}t}}\right]\right\} \quad L < x \tag{1.24}$$

where the term $[1-\gamma exp(-2\sigma L)]$ was expanded in a binomial series before performing the inverse transform.

1.2.3 Example of the classical heat conduction result

To model the experimental results considered in this thesis, the film is set to be 100 nm Cr film directly on top of bulk GaAs. An initial laser fluence of 14.88 mJ/cm^2 is used to provide the initial temperature jump in the film,

$$T_0 = \frac{F}{C_{film}L\rho_{film}} \tag{1.25}$$

where F is the absorbed laser fluence, C_{film} is the specific heat of the film, L is the length of the film, and ρ_{film} is the mass density of the film. All constants used in the thermal diffusion calculation are shown in Tables 1.1 and 1.2. Results are shown in Fig. 1.1. Although only four time points are shown in this figure, the complete

thermal profile (to a depth of 10 μm) was calculated at 10,000 depth points for each of the 753 time points recorded in the experiment, ranging from 30 ps to 3.37 μs .

GaAs Thermal Properties			
Quantity	Symbol	Value	Unit
Mass Density	ρ_{bulk}	5320	kg/m^3
Specific Heat	C_{bulk}	330	J/(kg·K)
Thermal Diffusivity	α_{bulk}	3.10×10^{-5}	m^2/s
Thermal Conductivity	k_{bulk}	55	W/(m·K)

Table 1.1: Values used for calculating thermal transport in the Gallium Arsenide bulk substrate. Note that $\alpha = k/\rho C$.

Cr Thermal Properties			
Quantity	Symbol	Value	Unit
Thickness	L	1×10^{-7}	m
Mass Density	ρ_{film}	7190	kg/m^3
Specific Heat	C_{film}	460	J/(kg·K)
Thermal Diffusivity	α_{film}	3.3521×10^{-5}	m^2/s
Thermal Conductivity	k_{film}	111	W/(m·K)

Table 1.2: Values used for calculating thermal transport in the Cr film.

1.3 Nanoscale thermal transport and the phonon mean free path

Microscopically, heat is transferred by quanta of vibrational energy called *phonons*. Phonons are treated using a kinetic model, analogous to the kinetic theory of gasses. In the kinetic model of gasses, energy is transferred by collisions between individual gas molecules, which occur on a characteristic collision time that depends on the density and temperature of the gas. This characteristic collision time can also be thought of as an average length between collisions, termed the mean free path (MFP). For a phonon gas, like a gas of molecules, the repeated exchange of energy following many collisions results eventually in a Maxwell-Boltzmann distribution of energy at equilibrium, and permits the definition of a temperature. The difference between these microscopic and macroscopic regimes can be seen in Fig. 1.3

Intuitively, heat is transferred faster by phonons that have larger MFPs. The Maxwell-Boltzmann distribution implies that there is an broad spectrum of phonon energies at finite temperature. Intuitively, the longer MFP phonons should conduct heat faster (longer MFPs means heat will travel farther before coming to a stop). Constraining a new phonon population to have a restricted energy spectrum might therefore be expected to alter thermal conductivity. In the experiment studied in this thesis, this restriction of phonon spectrum is accomplished by heating only a thin metal film, thereby limiting the production of long wavelength (and therefore low energy and large MFP) phonons, since *the film cannot support vibrational modes (phonons) that are larger than its physical size.*

Considerable theoretical efforts have been undertaken to understand how restricting the available thermal transport channels by limiting phonon spectra alters thermal conductivity [3]. One example calculation [20] is shown in Fig. 1.2, which shows longer phonon scattering lengths are required to reach thermal conductivities approaching bulk values.

To date, none of this depth dependence has been directly observed; the ultimate goal of this work is to perform temperature depth profile measurements to compare with those given in Fig. 1.1 and eventually more sophisticated models that can account for finite size effects, such as the Lattice Boltzmann Model [2].

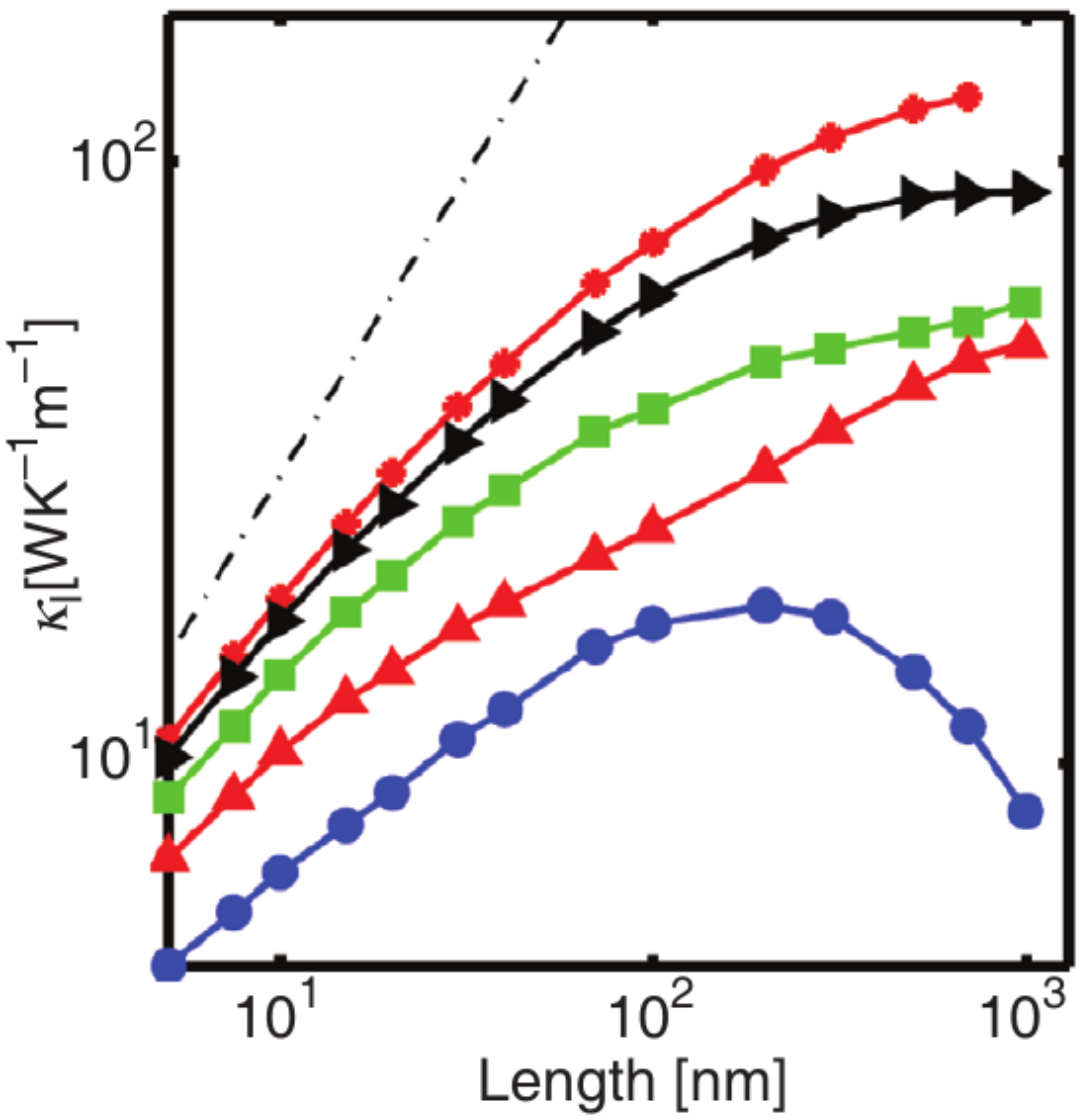

Figure 1.2: A calculation of thermal conductance vs. length, with each curve representing a different channel length (channel length is the width of the graphene nanoribbon that the phonon MFP travels along). Red circles have a channel length of 5 nm, black triangles a channel length of 4 nm, green squares a channel length of 3 nm, red triangles a channel length of 2 nm, and blue circles a channel length of 1 nm. The dashed line is unit slope. Taken from Aksamija (2017).

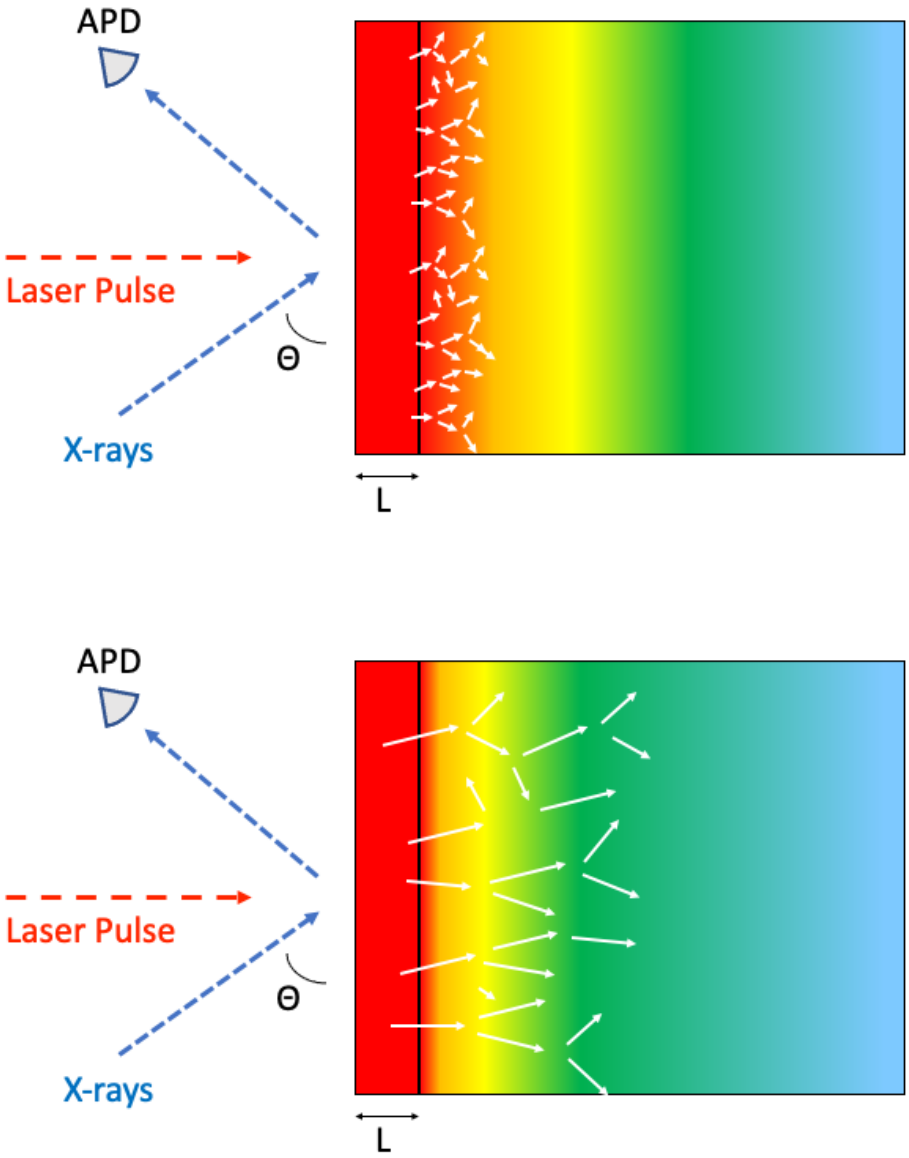

Figure 1.3: Pictured above are examples of fourier (top) and ballistic heat transport, as we would expect to see in our experimental setup. Notice that in the case of fourier heat transport, L is longer than the phonon MFP, whereas L is about the same length as the phonon MFP is the case of ballistic heat transport.

CHAPTER 2

Benchmarking diffraction calculations

2.1 Chapter introduction

The first major project of this thesis was checking a new x-ray diffraction calculation program (*TRXD*) against an existing set of tools (*GID_SL*). Tracking thermal transport throughout a crystal requires making not just a single, high-resolution recording of an x-ray diffraction pattern, but instead recording an entire sequence of such patterns. For phenomena such as thermal transport which cover many orders of magnitude in time (ps to μs), a large number of individual diffraction patterns must be analyzed in order to stitch together a stop-frame animation of the temperature profile evolution. This requires a new, efficient, program; *TRXD* was developed by DePaul University for this purpose. Here I explain the purpose of *TRXD* and benchmark its results against a standard software package, *GID_SL*.

2.2 X-ray diffraction as a temperature probe

When x-rays of wavelength λ are incident upon a crystal with lattice spacing d, significant x-ray reflected intensity is found only when the incident angle Θ with respect to the lattice planes satisfy the condition

$$n\lambda = dsin(\Theta) \tag{2.1}$$

where n is the order number of the diffraction peak. This is known as the *Bragg Law of Diffraction*. Taking the differential of Bragg's Law yields a method for measuring

small relative changes in lattice spacing $\Delta d/d$, or *strain*,

$$\frac{\Delta d}{d} = -\Delta\Theta cot\left(\Theta_B\right) \tag{2.2}$$

where $\Delta\Theta$ is a small angular shift away from the Bragg angle Θ_B that exactly satisfies Bragg's Law. For materials with a linear thermal expansion coefficient α_t, the change in position of a diffraction peaks may be used to calculate a temperature change ΔT,

$$\Delta T = -\frac{\Delta\Theta}{\alpha_t} cot\left(\Theta_B\right). \tag{2.3}$$

2.3 Dynamical diffraction

Bragg's Law is a consequence of *Kinematic diffraction theory*, which is the appropriate method applied when dealing with a small, short range order crystal that is imperfect. In the kinematic approximation, each cell in the crystal is treated as being independent, the x-rays are treated as plane waves, and the diffracted electric field amplitude can be found from

$$E_{diff} = E_i F \sum_L e^{2\pi i \mathbf{G}\cdot\mathbf{A}_L}, \tag{2.4}$$

where E_{diff} is the diffracted wave, E_i is the incident wave, $\mathbf{F}$ is the structure vector, $\mathbf{G}$ is the reciprocal lattice vector, $\mathbf{A}$ is a unit vector, and L refers to each individual unit cell. In one dimension, the condition for maximum diffracted electric field reduces to Bragg's Law. Within the kinematic approximation, the amplitude of the diffracted electric field can be decreased as a result of photoelectric absorption.

Calculating diffraction from crystals that are larger and more uniform (or "perfect") requires the use of a more involved theory called *dynamical diffraction*. Crucially, dynamical diffraction does not make the assumption that all of the cells in our crystal are independent. When we use the Darwin-Prins model of dynamical diffraction [21], there is a range of angles where the reflected intensity is relatively close to the incident intensity, and the diffraction peaks are no longer delta-functions near Θ_B.

This relative reflection may be angularly asymmetric. The finite width is due to the extinction effect, in which dynamical diffraction theory predicts that near strong reflections, electric field is reduced as energy is reflected outwards rapidly as the beam penetrates into a material. This results in a reduced number of crystal periods and limits the exactness with which lattice spacing can be precisely determined by measurement at one point. Despite this complexity, however, careful analysis of the diffraction peak lineshape can be used to extract depth-dependent lattice information, since the diffracted electric field varies throughout the crystal up to this extinction depth.

2.4 Dynamical diffraction calculations

A standard way of calculating x-ray diffraction peak lineshapes from strained crystals in the dynamical diffraction regime is using the *GID_SL* codes [22, 23]. Unfortunately these are closed-source, server-based programs that do not lend themselves to solving thousands of diffraction peaks for each sample studied, as required by time-resolved studies. Furthermore, the "SL" designation indicates that original development was for "superlattices", or periodic arrangements of strained crystals that are fabricated, rather than for smooth strain profiles generated by temperature gradients.

To meet this need, DePaul University began the development of an open-source, efficient, portable software package named *TRXD* that is maintained in a public depository and is written in the MATLAB programming language [24]. It uses an alternative algorithm to the one used by *GID_SL*, first described in [15], but with an adaptive step size in depth that allows the code to handle rapidly changing strain profiles while retaining computational accuracy. The underlying calculations are written in matrix form and are vectorized by treating each $\Delta\Theta$ individually. Additional computational efficiency is found by using logical array operations to perform square root operations in the complex plane. An outline of how *TRXD*

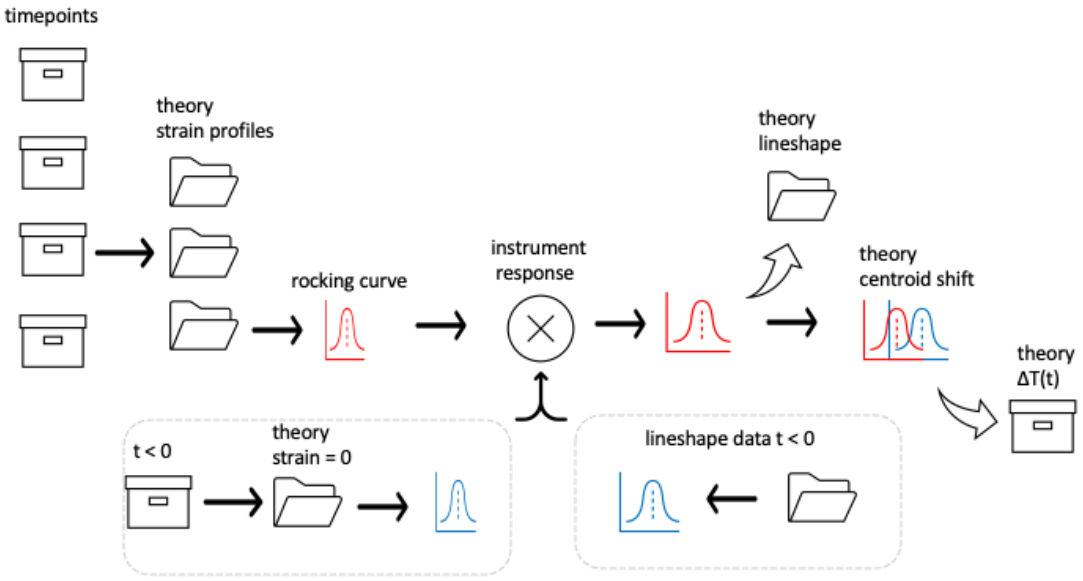

Figure 2.1: Data analysis and modelling procedure. We begin by putting our information into *TRXD* (timepoints, angular ranges for rocking curve calculations, material constants, and laser fluence), which produces strain profiles that are used in turn to find the rocking curves expected from the classical model. Next the centroids are compared to the rocking curve data collected before time zero, which is used to determine the average temperature change using the thermal expansion coefficient.

works can be found in Fig. 2.1

2.5 Code benchmarking

Several different comparisons were made between *TRXD* and *GID_SL*, both for bulk GaAs with the same reflection order and at the same x-ray energy of 10 keV used in experiments. The output of each code was formatted as a *rocking curve*, or the result that would be obtained as a perfect crystal is slowly rocked along Θ near the Bragg diffraction peak, while the peak of the total diffracted intensity was recorded as a function of angle. Benchmarks included unstrained GaAs, or $\Delta d/d = 0$ everywhere, and various uniform strain levels, or $\Delta d/d = constant$. Both

codes were run independently, and the results manually imported and overlapped. No disagreement was found for GaAs at 10 keV, or for the similar semiconductors Ge, Se, or InSb also used in the larger study at this x-ray energy.

To pull down results from the *GID_SL* server efficiently, a script was written in MatLAB (see Appendix) that could take an arbitrary depth-dependent strain profile, such as one generated by the classical thermal diffusion model demonstrated in Fig. 1.1, and break it down into small strain layers for *GID_SL* to calculate. Although helpful in getting the codes to behave similarly, it proved to be very time-intensive for the server since a large number of discrete strain points are needed to recapitulate the smooth strain profile calculated by application of the Fourier Law.

Instead, a different approach was taken: to see if *TRXD*'s adaptative step size technique could handle the abrupt change of a single sharp buried strain level, a situation that *GID_SL* was designed to handle. Fig 2.2 shows the result of a calculation of a strain step-function where $\Delta d/d = 10^{-4}$ over the first 2 μm of the surface, with the remainder of the bulk crystal unstained. The unstrained rocking curve is shown for reference, and was identical for both curves. *TRXD* shows the overall rocking curve slightly shifted, an effect which is not understood, but which does not concern us as the shift is small enough to be negligible. The shape however is otherwise identical. Fig. 2.3 shows the same result, but on a logarithmic intensity scale.

In addition to quantitative agreement, the results agree with expectations. The unstrained rocking curve calculation peaks near the calculated Bragg angle of 26.02 degrees, with an intensity just below unity due to a small amount of photoelectric absorption. The curve is narrow, with an intrinsic width near one millidegree. In the strained crystal curves, the largest peak is due to the same unstrained substrate, which is present within the x-ray probe depth of a few microns. This peak is only slightly distorted, but reduced in intensity. The large secondary peak shifted to smaller angles corresponds to a positive strain. The peak separation agrees with

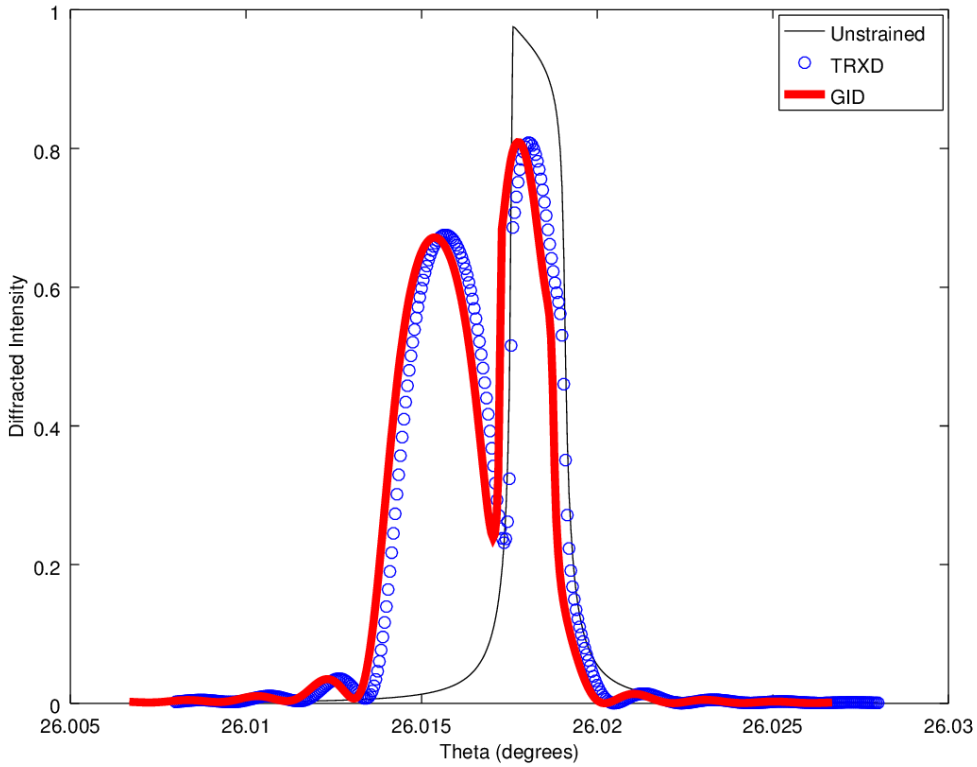

Figure 2.2: Linear scale comparison of *TRXD* and *GID_SL* for a test case of 0.01% uniform strain over the first 2 μm of depth in GaAs [004] reflection at 10 keV. The unstrained crystal result is shown for reference.

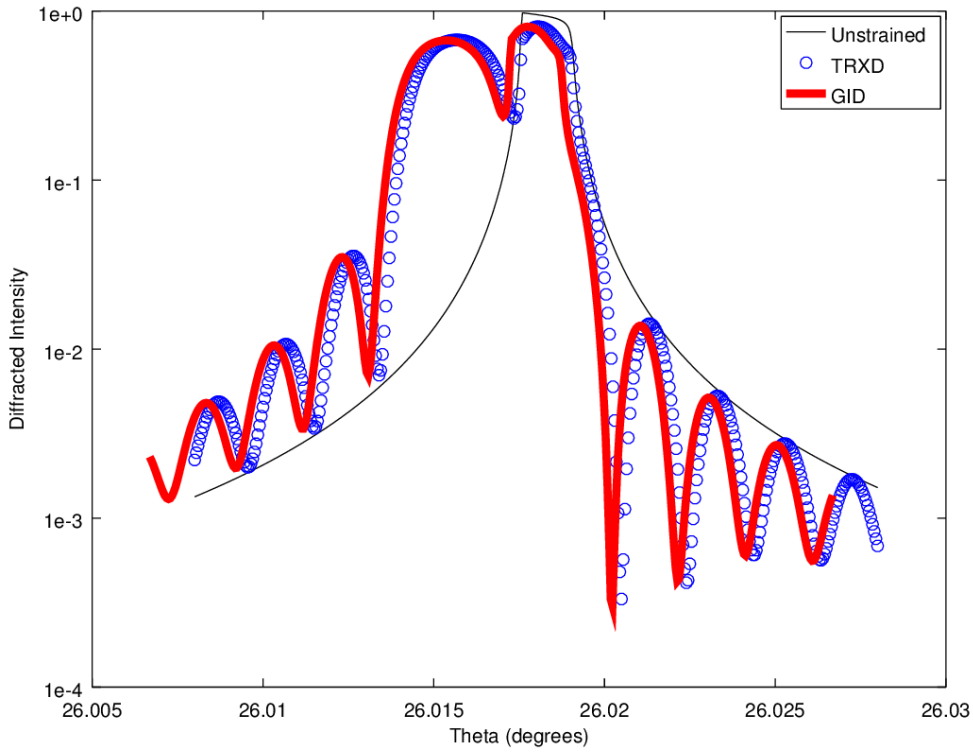

Figure 2.3: Linear scale comparison of *TRXD* and *GID_SL* for a test case of 0.01% uniform strain over the first 2 μm of depth in GaAs [004] reflection at 10 keV. The unstrained crystal result is shown for reference.

the differential form of Bragg's Law. Finally, the fringes (more clearly visible in the logarithmic plot) are due to interferences between the two distinctly strained layers, with their periodicity given by the strain within our 2 μm depth of our GaAs.

This level of agreement between the new, DePaul-developed *TRXD* and the widely used code *GID_SL* demonstrate that *TRXD* can be used for analysis of x-ray rocking curves for the [004] reflection in GaAs at 10 keV.

CHAPTER 3

Comparison to experiment

3.1 Chapter introduction

The second major project of this thesis was comparing rocking curves calculated by the new software *TRXD* with experimental data. This chapter reviews how the data was collected, describes the data reduction process, and demonstrates the use of a Voigt profile to match the angular resolution of experiments with the dynamical diffraction simulation for comparison.

3.2 Time-resolved x-ray diffraction experiment

Data was collected prior to when I joined the research group by members of Dr. Landahl's research group and collaborators, using beamline 7ID of the Advanced Photon Source at Argonne National Laboratory. Details of the data collection approach are shown in Fig. 3.1, taken from [14]. Monochromatic 10 keV synchrotron X-rays (blue) pass through a scattering foil on their way to a sample which is rocked in small steps across a small angular range near a Bragg peak. The proportional mode Avalanche Photodiode (APD) collects all x-rays from the diffraction curve, and has its signal averaged and recorded by an oscilloscope. The x-rays are produced in 100 ps long bunches separated by 153 ns, and synchronized to an external 50 fs amplified laser pulse (red) that has a pulse repetition frequency of 1 kHz. The laser triggers the oscilloscope acquisition, which averages for 1000 laser shots before saving an APD trace. The timing delay between the laser and x-rays can be arbitrarily adjusted. The laser also strikes the sample (not shown), focused to ≈ 0.1

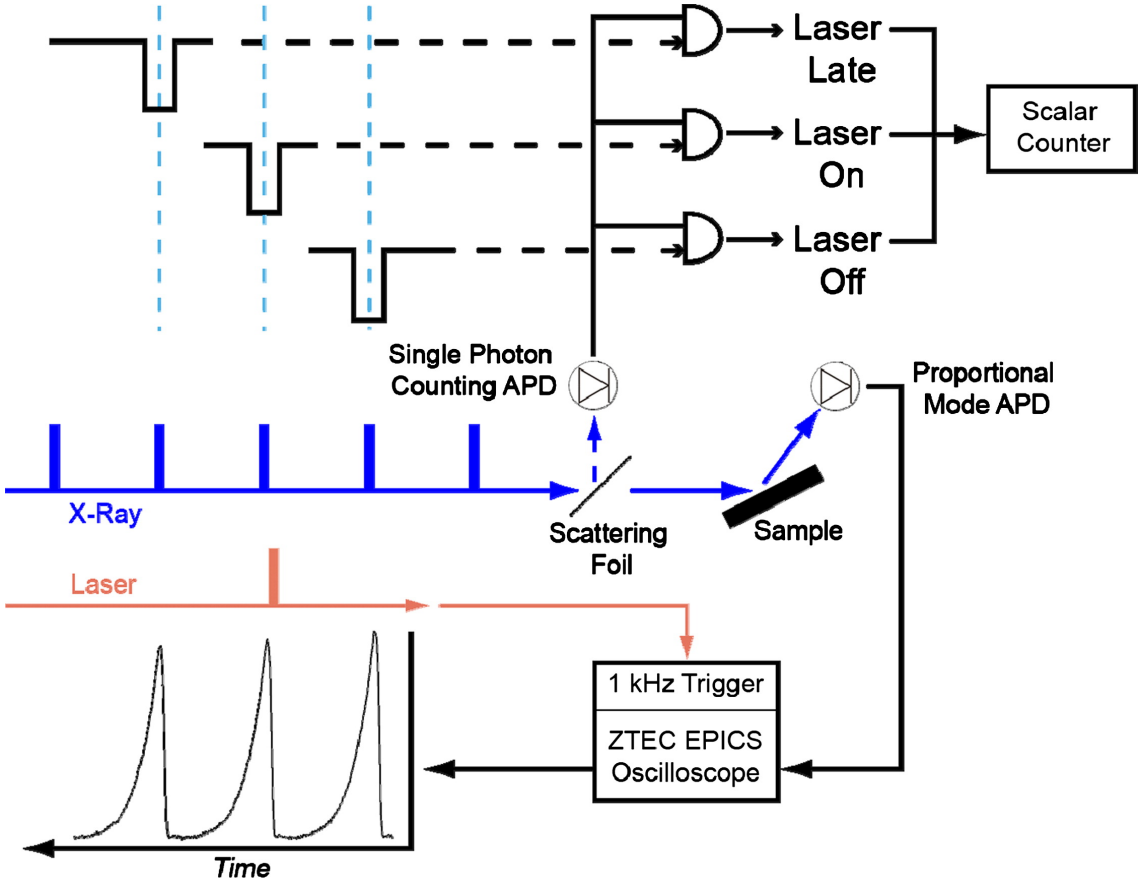

Figure 3.1: Data collection for time-resolved diffraction measurements used in this thesis. See the text for full description; taken from *Williams (2011)*.

cm^2 to overlap the x-ray spot size of ≈ 50 μm (Vertical) $\times$ 500 μm (Horizontal) on the ≈ 1 cm^2 sample. Usually a scattering foil is used to generate a time-resolved normalization signal by producing a signal that reproduces the uneven fill pattern of the synchrotron; this typical approach was not used in this data set due to the need to record very long time-series to follow diffusion process. A different normalization process using prior bunches with the proportional mode APD was used instead.

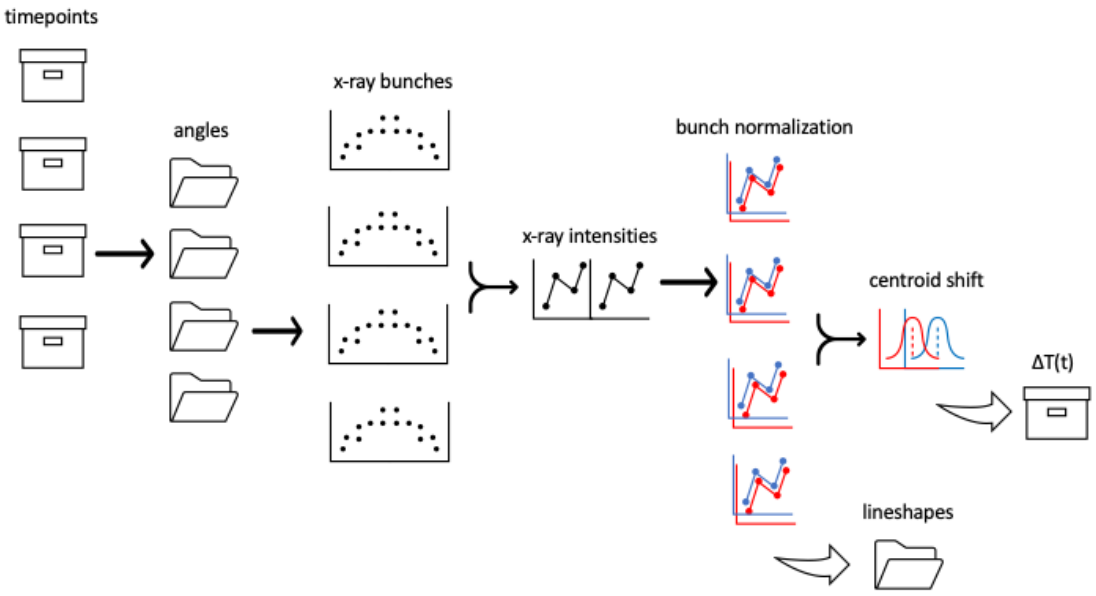

Figure 3.2: A flowchart picturing how data was extracted (code is attached in the Appendix). From a set of desired time delays, a range of angles covering a rocking curve are collected with x-ray bunches both before and after the laser strikes the sample. Intensities are extracted from oscilloscope traces using SLM and then normalized using the same x-ray bunch from the preceeding storage ring revolution. These intensities are plotted against the rocking curve angular range to give lineshapes that will be compared to those calculated using a Fourier Law model and *TRXD*. A compact representation of the data is made by calculating the centroid shift from the rocking curves that we can use to find the average temperature change of the bulk material region probed by the x-rays.

3.3 Data reduction

An outline of this section can be found in Fig. 3.2. Oscilloscope traces were recorded for 151 angular points, from 27.189 degrees to 27.3090 degrees in 1 millidegree steps across the Bragg peak (27.2489 degrees at 10 keV) at each time delay. An example oscilloscope trace is shown in Fig. 3.3. Each x-ray pulse creates a negative voltage ($\approx$ -35 mV in this case), and overshoots to a positive voltage ($\approx$ +10 mV in this case) before the next pulse. The synchrotron storage ring was in the standard 24 bunch fill pattern: each 100 ps duration x-ray bunch is separated by 153 ns, with the total revolution time being 3.68 μs.

On the edges of the rocking curve, the x-ray intensity will be much smaller. Fig. 3.4 shows an oscilloscope pattern at nearly 1000 times smaller x-ray intensity.

Each oscilloscope trace was acquired by averaging for 1,000 laser shots, or one second. For each averaged oscilloscope record, 10,000 samples were taken across just over two storage ring revolutions, which would be 48 bunches in 7.36 μs. This means there was approximately one sample per nanosecond, or 150 samples per x-ray bunch. An example of three consecutive x-ray bunches is shown in Fig. 3.5 with each individual oscilloscope sample represented as a point. The x-ray bunches recorded are much longer than their 100 ps duration, due to the limited bandwidth of the APD and the oscilloscope.

The Advanced Photon Source synchrotron operates normally in a "top up" mode where the individual bunches are routinely filled with more charge to make up for scattering losses. This refilling is done to maintain average beam current stability, but results in significant bunch-to-bunch current fluctuations. This is evident in the oscilloscope trace in Fig. 3.3 which shows considerable variability between each bunch. This is the purpose of acquiring at least two complete storage ring revolutions: the x-ray intensity in a given bunch does not change in a single revolution, so the earlier revolution can be used to normalize away these bunch intensity fluc-

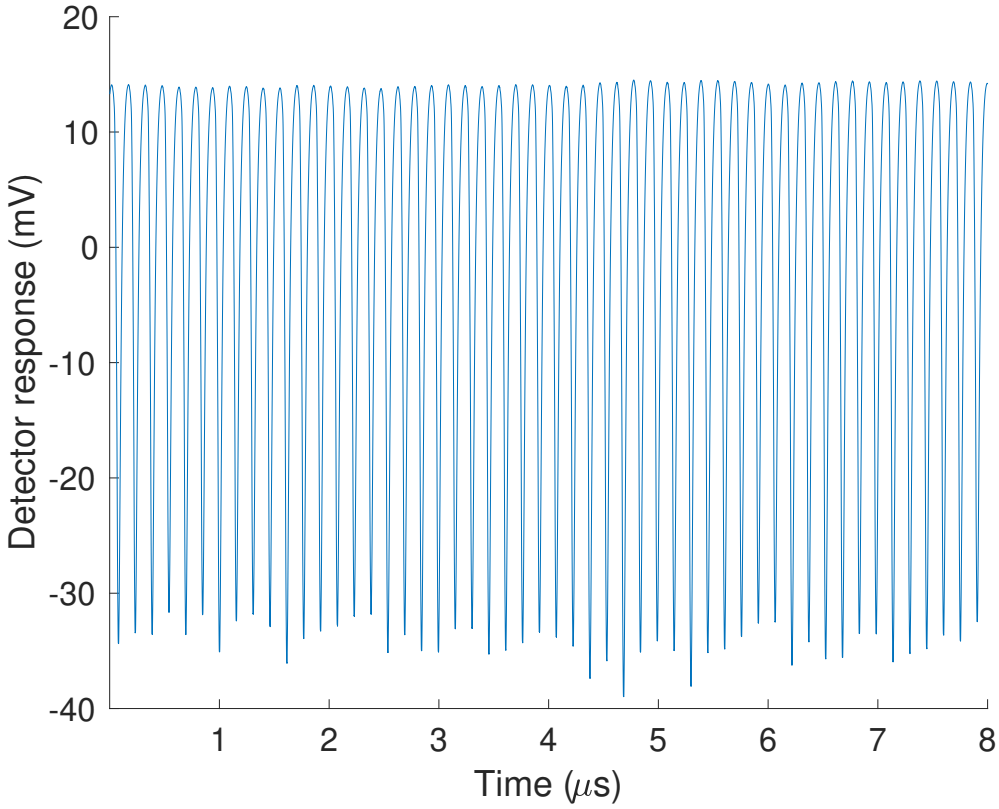

Figure 3.3: Avalanche Photodiode (APD) detector response to just over two storage ring rotations (the data was taken twice - once with and once without the laser heating our sample) in the standard 24 bunch operating mode. This data was recorded following diffraction from a laser-excited sample, near the peak of the Bragg diffraction peak.

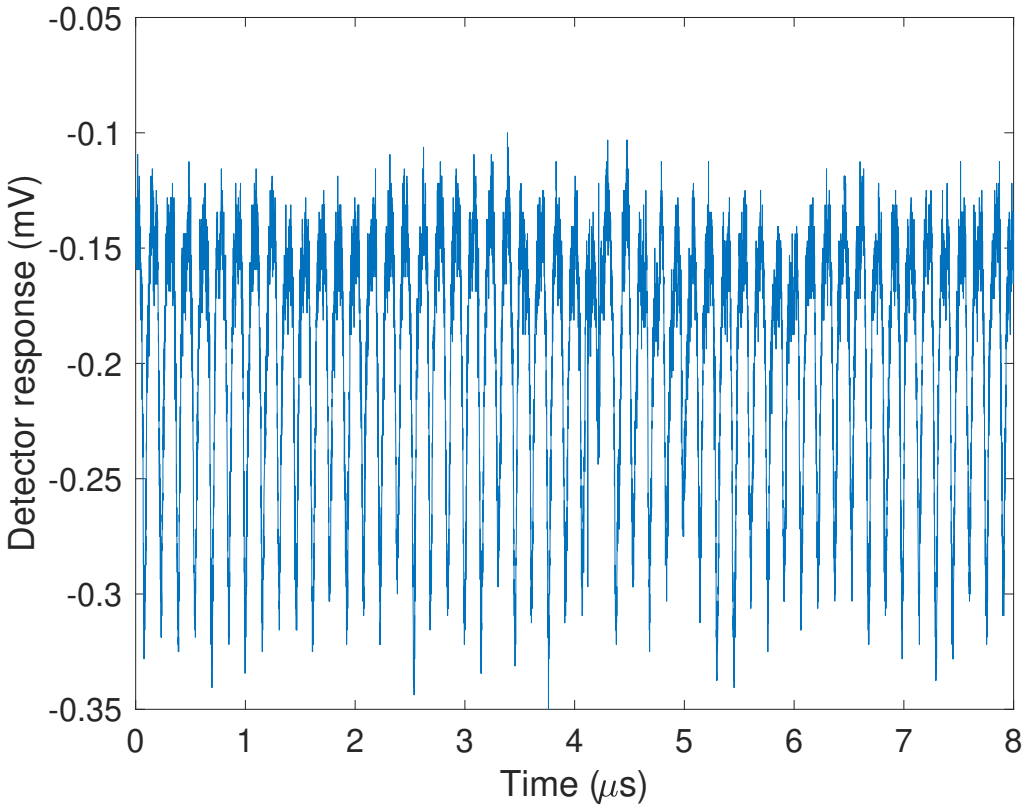

Figure 3.4: APD response from just over two storage ring rotations, but at low intensity far away from the Bragg diffraction peak.

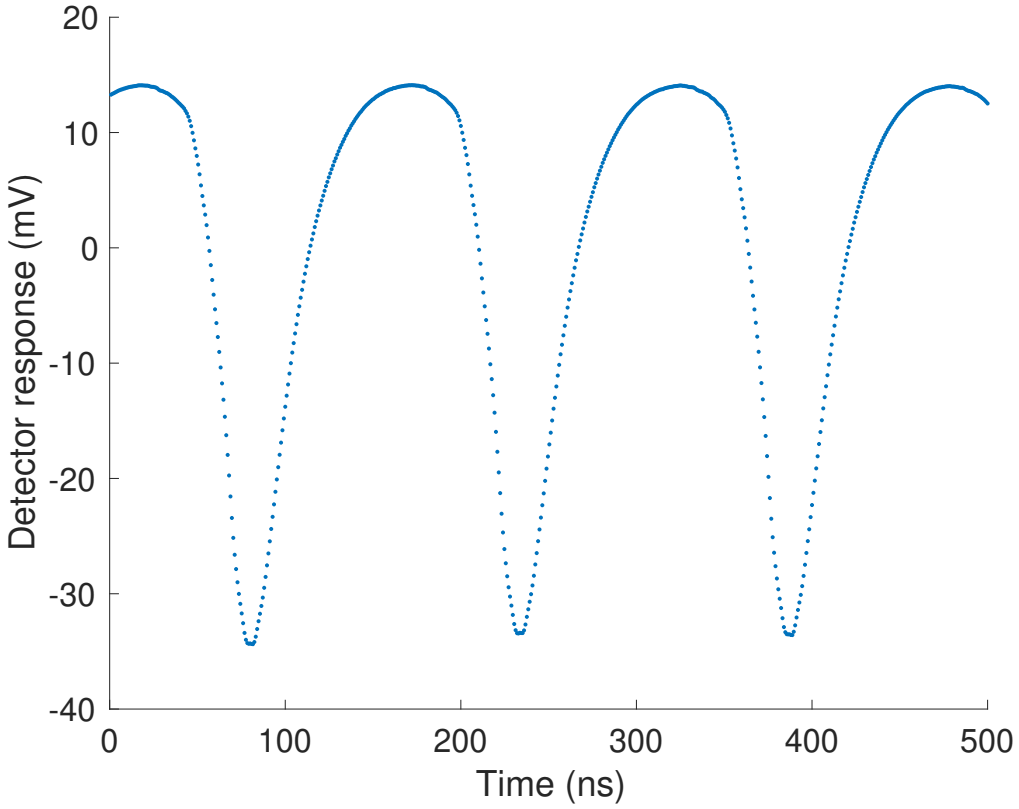

Figure 3.5: APD response from only 3 bunches, showing individual oscilloscope samples as points. Approximately one sample is taken every nanosecond, with 153 ns between x-ray bunches in the standard 24 bunch mode of the APS.

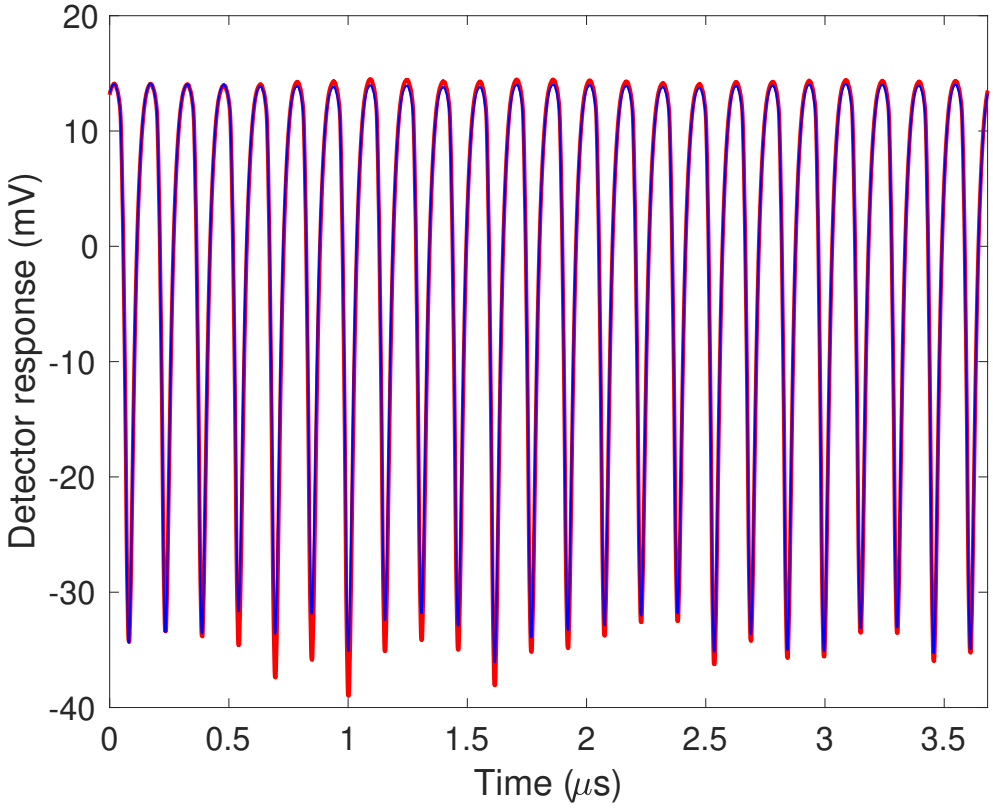

Figure 3.6: APD response from two consecutive storage ring rotations overlapped. The later revolution is shown in red, the earlier pre-laser revolution is in blue. The laser strikes the sample, altering x-ray diffraction intensity just before the fourth bunch. Thermal recovery is observed over several μs as the red and blue curves approach each other.

tuations. This is illustrated in Fig. 3.6 which shows the exact sample oscilloscope trace as Fig. 3.3, but with the second set of 24 bunches translated earlier in time by one ring revolution. The earlier bunches are in blue and the later bunches are superimposed in red. Although the total pattern looks noisy, in fact the first 3 bunches are seen to overlap nearly perfectly. The laser strikes the sample after the third bunch, and so the remaining bunches see a difference in x-ray intensity. It is this comparison method that allows for very small changes in x-ray intensity, and therefore very small changes in x-ray rocking curve position (and therefore Bragg angle shift and ultimately temperature changes) to be recorded.

The next data reduction step is extracting an x-ray intensity from the trace of each bunch. The APD pulses are created by charges generated by the absorption of x-rays in the detector, which is then amplified via both internal processes (avalanching) and external electronic high-speed amplifiers. Therefore, with a fixed time response, either measuring the pulse height or area under each curve should give a measurement of x-ray intensity. The changing overshoot (recovery) of the proportional mode detector makes this difficult. Therefore the research group has been developing a new analysis method based on *Shape Language Modeling (SLM)*, demonstrated in Figs. 3.7-3.10. Note that the inverse of the raw data shown previously has been taken in these plots for clarity (so that each x-ray bunch now goes up with intensity). SLM uses constrained piecewise continuous cubic spline interpolation to model arbitrarily shaped data, and is available as a MatLAB package [25]. As shown in Fig. 3.7 for higher x-ray intensity data samples (blue circles), "knot" locations (vertical green dashed lines) are chosen as fixed locations where the cubic splines are joined. Additional constraints are applied in this SLM, such as requiring monotonic rising behavior before the peak and falling behavior following the peak. The SLM curve (red line) therefore provides an appropriately smoothed empirical fit to the data, allowing the minimum and maximum peak height to be extracted while using the entire sample set across the peak.

The utility of this approach is demonstrated in Fig. 3.8, which is from an x-ray bunch recorded at a lower intensity region of the rocking curve. Selecting just the minimum and maximum of the data in this region is sensitive to noise at these low signal levels, and subtracting the extrema would result in an overestimate of x-ray intensity. Fig. 3.9 shows the ability of SLM to extract x-ray intensities that are only 40 μV in height, implying that a dynamic range of over 3 orders of magnitude can be obtained in this time-resolved measurement when compared with Fig. 3.7. Finally, Fig. 3.10 shows that the SLM data extraction method can begin to fail when the intensity gets low enough, with the x-ray intensity likely over-estimating differences between a peak and signal that may not actually exist.

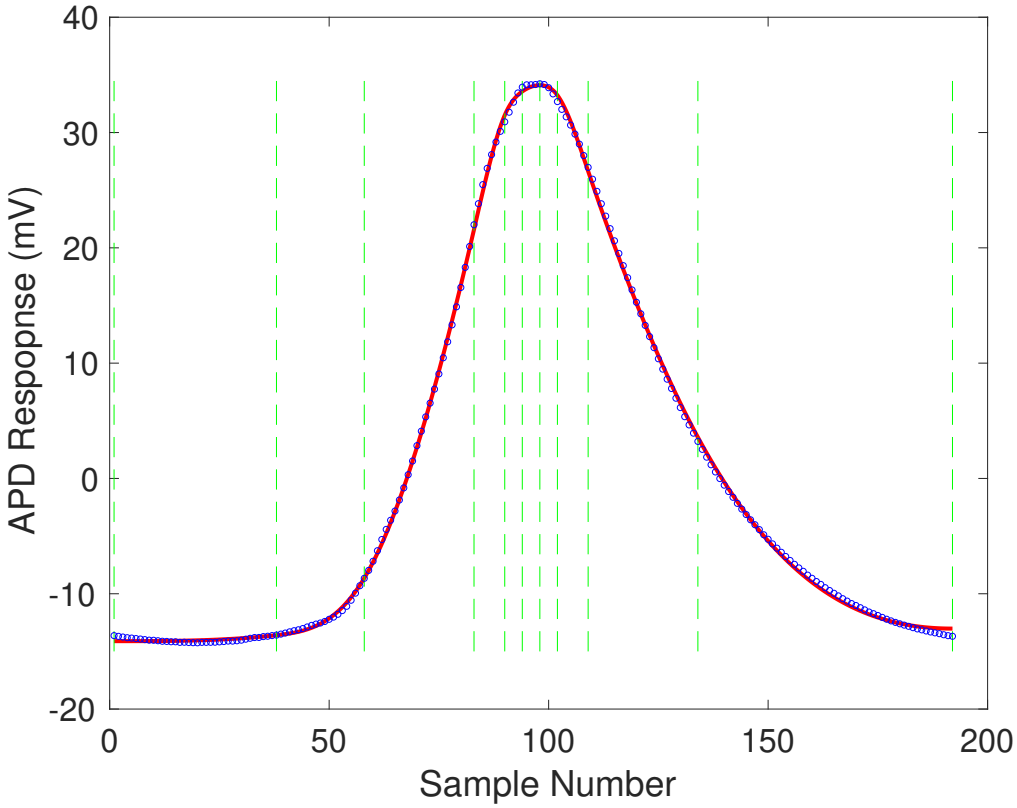

Figure 3.7: Fitting the inverted APD response (blue points) to a single x-ray bunch at relatively high x-ray intensity using SLM (red line). Knot locations where cubic splines are tied together are shown as dashed green lines.

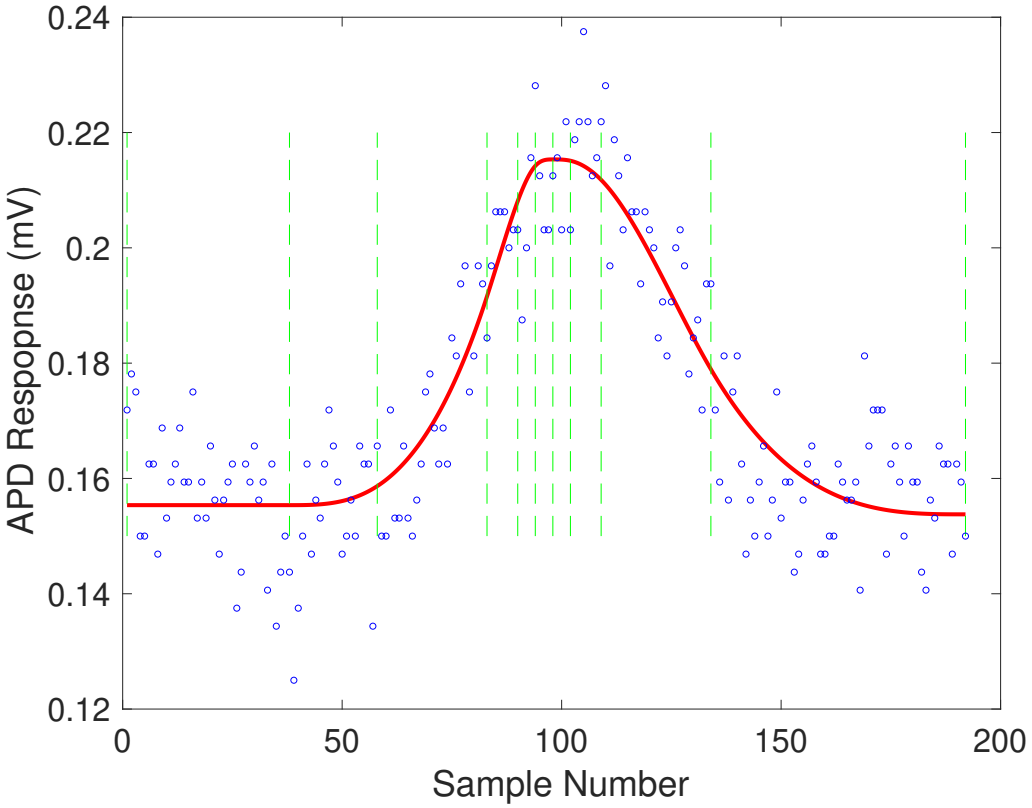

Figure 3.8: Fitting a the inverted APD response (blue points) to a single x-ray bunch at relatively low x-ray intensity using SLM (red line). Knot locations are the green dashed lines.

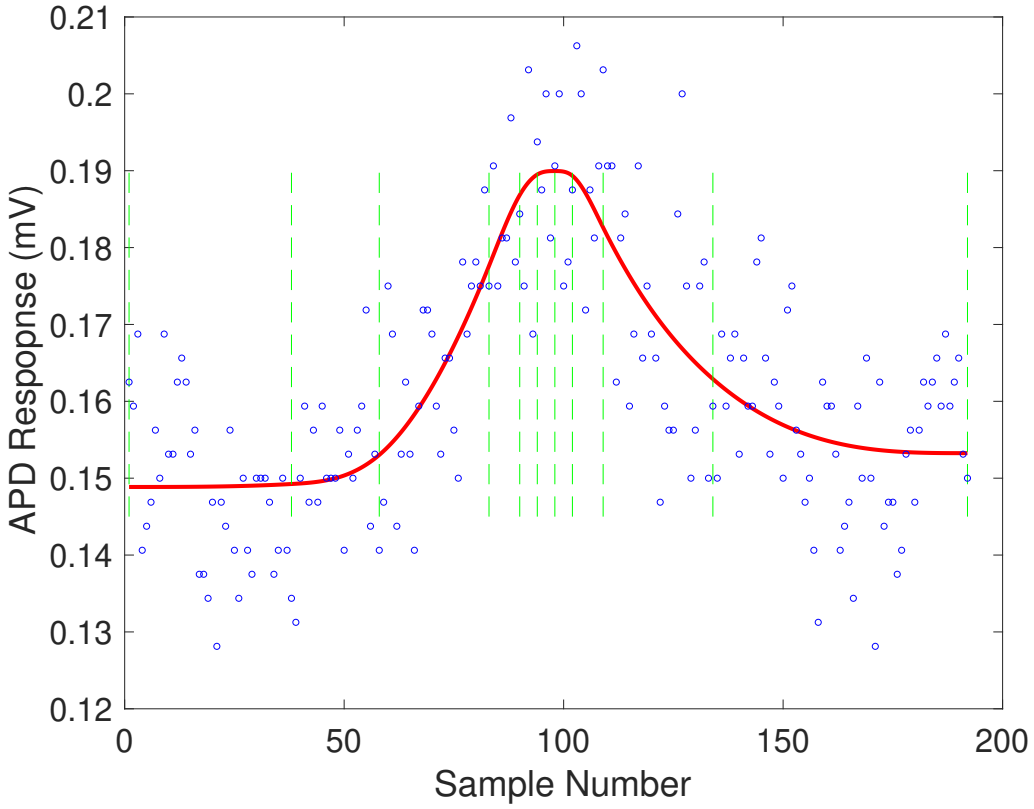

Figure 3.9: Fitting the inverted APD response (blue points) to a single x-ray bunch at very low x-ray intensity using SLM (red line). Knot locations are the green dashed lines. High noise levels would cause overestimation of extrema difference without SLM-assisted data smoothing.

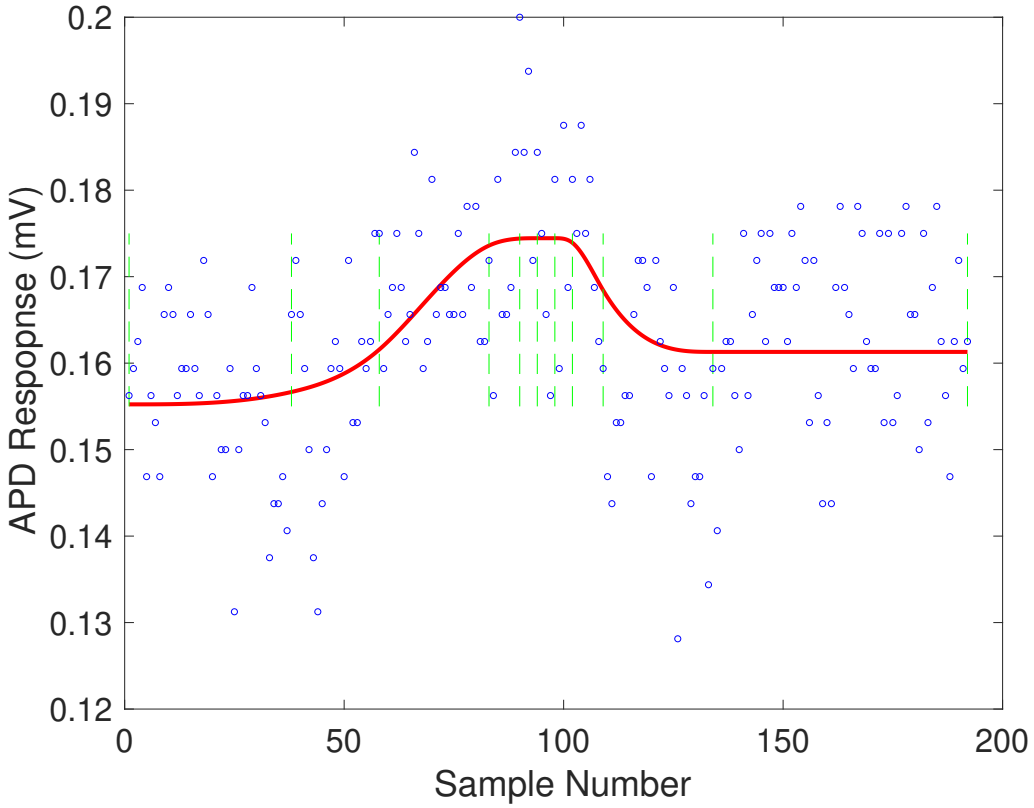

Figure 3.10: Fitting the inverted APD response (blue points) to a single x-ray bunch at vanishingly low x-ray intensity using SLM (red line). Knot locations are the green dashed lines. SLM likely causes overestimation of a signal that is buried in noise.

3.4 Convolution with instrument resolution

The dynamical diffraction peak shapes calculated using either *TRXD* or *GID_SL* represent an ideal experimental situation where the incident x-ray beam has no energy spread or angular spread, and the unstrained GaAs substrate is truly perfect. All of these effects add blurring to the rocking curves. To account for the loss in resolution, each calculated rocking curve is convolved with a normalized Voigt profile,

$$I_{meas}(\Theta) = \int_{-\infty}^{\infty} V(\Theta') I_{calc}(\Theta - \Theta') d\Theta' + I_0 \tag{3.1}$$

where $I_{calc}(\Theta)$ is the calculated rocking curve intensity from *TRXD*, I_0 is a constant offset to compensate for the overestimation of extremely small signals due to SLM as described in Fig. 3.10, and $I_{meas}(\Theta)$ is the anticipated measured rocking curve following convolution with the instrument response function described as a Voigt curve V,

$$V(\Theta) = \int_{-\infty}^{\infty} G(\Theta') L(\Theta - \Theta') d\Theta' \tag{3.2}$$

which is itself a convolution of a Lorentzian lineshape,

$$L(\Theta) = \frac{\gamma}{\pi\left(\Theta^2 + \gamma^2\right)} \tag{3.3}$$

with a Gaussian lineshape,

$$G(\Theta) = \frac{e^{-\Theta^2/\left(2\sigma^2\right)}}{\sigma\sqrt{2\pi}}. \tag{3.4}$$

The Lorentzian width, γ, Gaussian width, σ, and fixed offset, I_0 are all free parameters chosen to overlap the calculations for unstrained data with the measurement of the unstrained crystal sample, taken from the x-ray bunch before the laser strikes the sample, i.e. when $t < 0$. The success of the Voigt profile in matching the experiment to the data is shown in Fig. 3.11, and is subsequently applied to all other strained rocking curves, prior to intensity normalization. A best fit to data was found with $\gamma = 0.35$ mdeg, $\sigma = 1.45$ mdeg, and $I_0 = 0.5\%$ of the maximum intensity. These are reasonable values given that the angular step size taken in the experiment was

only 1.0 mdeg, corresponding to the smallest angular step size that could be repeatably performed by the diffraction instrument. A function for efficiently convolving rocking curves with this instrument response is included in the Appendix. Future work may include modifying the Voigt profile with an asymmetric Lorentzian profile to better match the data. The success of *TRXD* in modeling unstrained x-ray diffraction data for this experiment indicates that study of thermal transport using the same data reduction and instrument resolution methods should be valid.

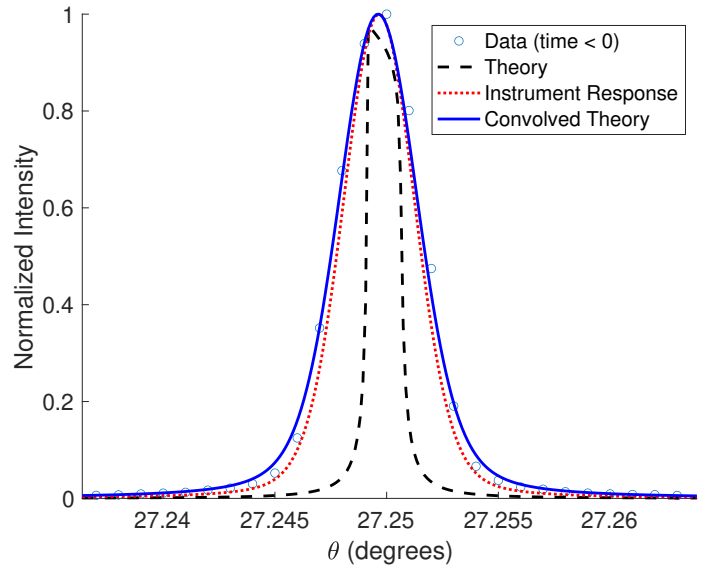

(a)

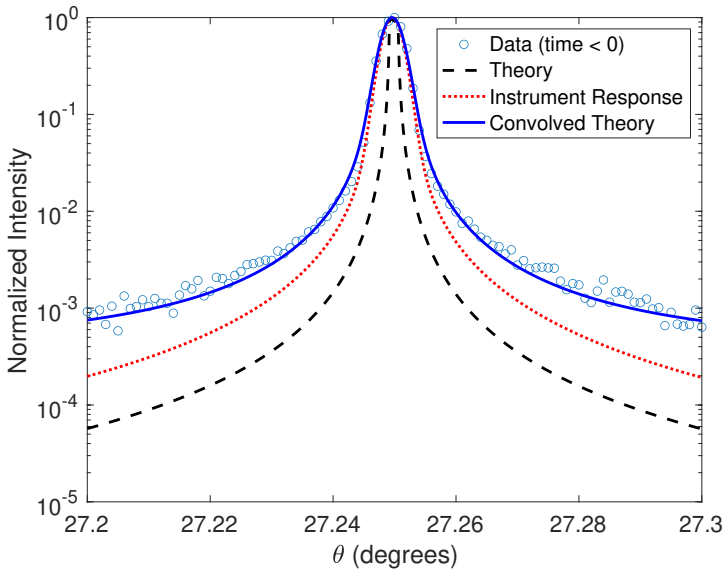

(b)

Figure 3.11: *TRXD* unstrained rocking curve theoretical calculation (dashed line), the Voigt profile instrument resolution function (dotted line), and the theoretical calculation convolved with the instrument resolution (solid line) compared with unstrained [400] GaAs rocking curve measurement at 10 keV (circles).

CHAPTER 4

Agreement and discrepancy with classical theory

The centroid of the diffraction peaks at each measured time delay was determined for both the classical thermal film model and the data, and subtracted from the measured centroid of the unstrained crystal (Bragg diffraction peak). **A single free parameter, the absorbed laser fluence, was adjusted to match experiment with data.** The results of the calculation are shown overlapped with the data in Fig 4.1. Data is collected before the laser strikes the sample (when $t < 0$) as a control, and is found to have zero shift from the unstrained measurements.

The behavior seen in Fig. 4.1 can mostly, but not entirely be explained by the classical thermal film model of Eq. 1.24. The first few tens of ps cannot be accurately observed, due to the x-ray bunch duration of 100 ps which would blur out the earliest and fastest movement of heat into the substrate. Although the temperature at the film/substrate interface is initially very high, as seen at 1 ns in Fig. 1.1, it has not diffused very far into the substrate and therefore only a small fraction of the x-rays within the penetration depth experience a diffraction peak shift, so the average centroid shift at first is small. This increases rapidly as the heat continues to flow into the x-ray probe depth, shifting the peak to lower angles in agreement with Eq. 2.3. After about 10 ns, the peak average lattice expansion is reached as the heat begins to flow out of the x-ray probe depth, and the surface of the crystal begins to slowly cool. The first several microns of the substrate have nearly reached the original temperature by 3.5 μs, when data collection ends. The crystal will have completely recovered before the next laser pulse re-heats the sample in 1 ms.

The theoretical curves show a very similar cooling rate past 100 ns. The small differ-

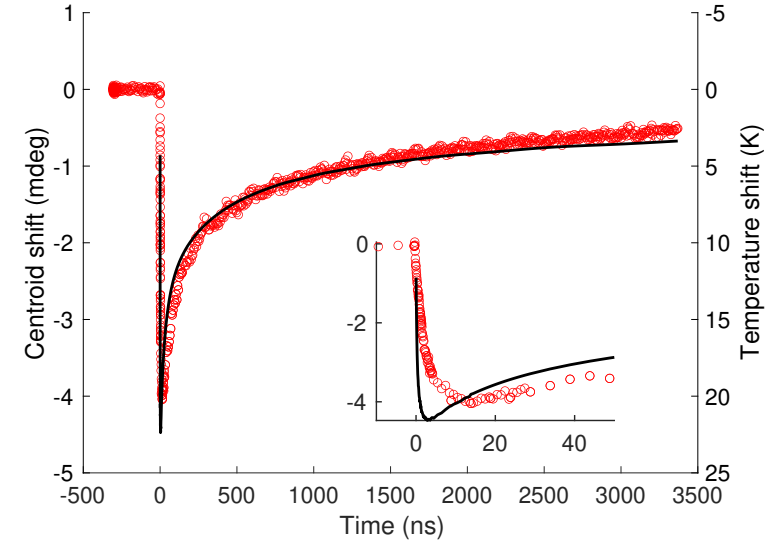

(a)

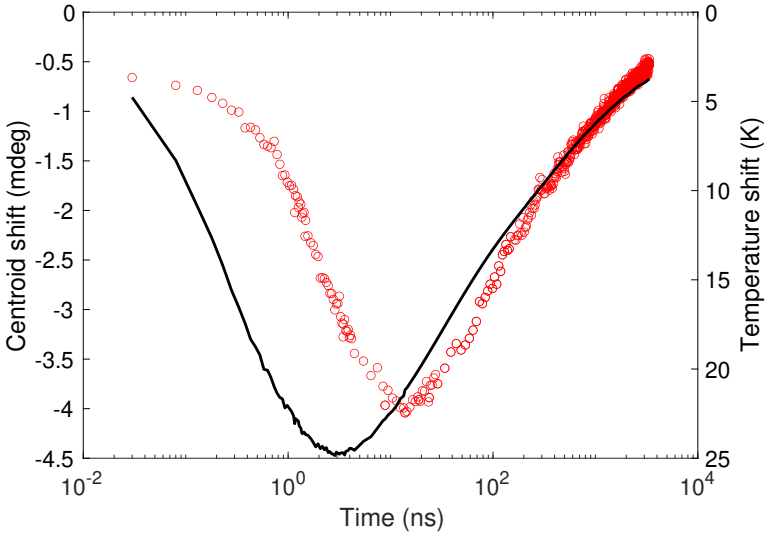

(b)

Figure 4.1: Classical thermal film model rocking curve centroids (calculated using *TRXD*, black line) and data (red circles) for a 14.88 mJ/cm^2 absorbed laser fluence on 100 nm thick Cr deposited on bulk GaAs at 10 keV. The top figure is linear in time, the lower figure is on a logarithmic time scale. The inset in the top figure shows data and model near $t = 0$. Temperature shifts are calculated from centroid shifts using Eq. 2.3.

ences observed may be due to the neglect of other thermal dissipation mechanisms not included in the model, such as lateral heat conduction (only a 1D model is used), or radiative heat off the surface. Unsurprisingly, the classical Fourier Law of heat transfer is found to qualitatively and quantitatively describe the data at long timescales, or when the heat has already spread over a macroscopic distance. The values of thermal conductivity for GaAs are well established, and this measurement is in agreement.

There is significant disagreement however at times below 100 ns. First, in order to match the long-timescale cooling, the maximum laser fluence had to be raised about 20% over value needed to reach the peak lattice displacement observed. This is most clear in the logarithmic time (lower) plot in Fig. 4.1, which shows a measured maximum negative centroid shift of -4 mdeg, but a corresponding simulation value of -4.5 mdeg. Second, the maximum angular shift occurs significantly earlier for the model than for the data. This is also clear from the inset in the upper figure, which shows a difference of close to 10 ns between theory and experiment.

This data, along with confidence in the TRXD simulation tool gained from the earlier chapters of this thesis, provides clear evidence for the central hypothesis of nanoscale thermal transport described in the first chapter: that heat conducts slower at short distances than in bulk materials. It takes longer to transmit from the 100 nm thick Cr film into the substrate than would be expected by classical theory, but after a few ns it behaves as predicted by Fourier the half-millimeter thick GaAs substrate. This observation confirms quantitatively the one made by the research group in 2007. Their main result is duplicated in Fig. 4.2 [11].

Notably, the heat impulses also arrive later in the data than in the simulation for the 2007 result, and also require a similarly higher laser fluence to match the peak position. This is remarkable given that the entire rocking curve shape was estimated from a single data point taken at the half-maximum of the diffraction curve, and

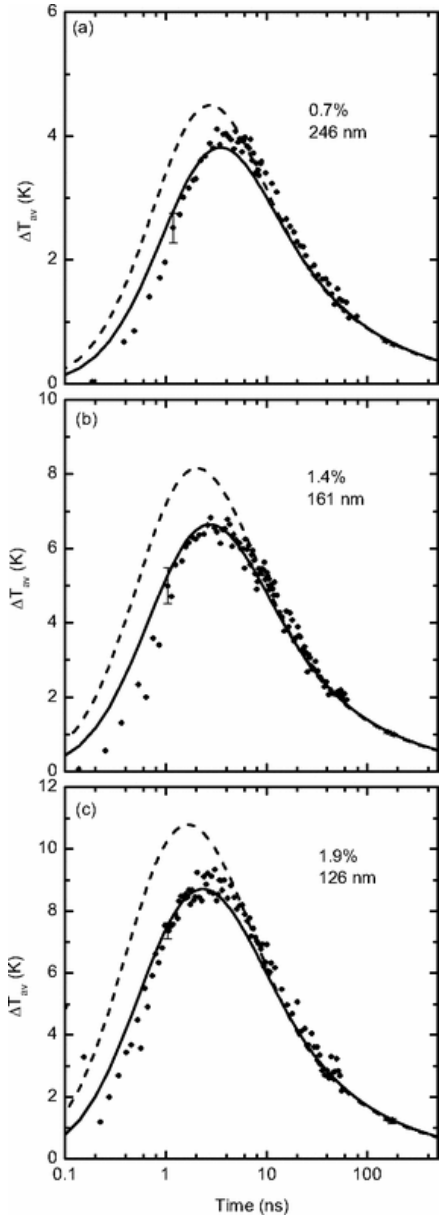

Figure 4.2: Previously published results by *Highland et al., 2007* using time-resolved x-ray diffraction to study a 100 nm metallic film on GaAs. The figure shows the time evolution of the average temperature of layer as determined from shifts of the diffraction peak, see Eq. (12) of *Highland*. The dashed lines are the evolution of the weighted average temperature of the buried layer predicted by a solution to the diffusion equation using the values of probe layers fabricated from InGaAs alloys of 246 nm, 161 nm, and 126 nm on top of the GaAs substrate but below the film. Dots are data, not from centroids, but deduced from a single data point located at the half-maximum of the rocking curve. Dashed lines are a classical thermal transport model, and the solid line was a two-channel model developed to describe the dataset.

that dynamical diffraction theory was not used in the interpretation of the result – only three separate depth probe heights were used at 246 nm, 161 nm, and 126 nm below the film. **Our results, analyzed with *TRXD*, are in strong agreement with this earlier published data and show similar discrepancies with the Fourier Law.**

Dynamical diffraction measurements and calculations however can tell a great deal more about exactly what happens to the missing heat, which could only be guessed at in *Highland et al.*. In that paper, the slowed cooling was attributed to a second thermal transit channel, containing about 20% of the total thermal energy, and resulting from "ballistic" phonon transport, i.e. transport events within a phonon MFP.

Now, however, we are able to see exactly what the diffraction patterns are at each measured timepoint, and compare them with a model that uses a benchmarked dynamical diffraction code to compare them with the detailed result of the classical simulation. A selection of representative high resolution rocking curve calculations and measurements are presented in Figs. 4.3 - 4.14 and are discussed in the next section.

4.1 Observed behavior

The first frame recorded after the laser strikes the sample, shown in Fig. 4.3, shows only a slight change in x-ray reflectivity that is primarily in the wings of the diffraction peak. Substantial changes in the diffraction peak shape appear within the first nanosecond, e.g. Fig. **??**. According to the Fourier Law model, the heat should diffuse into the sample a characteristic diffusion length of $L_D = \sqrt{4\alpha t}$. Using the value of the diffusivity, α, from 1.1, the temperature jump should have travelled 350 nm in the first 1 ns. This is also demonstrated in the calculated temperature profile shown in Fig.1.24 as the red curve. However the x-rays are

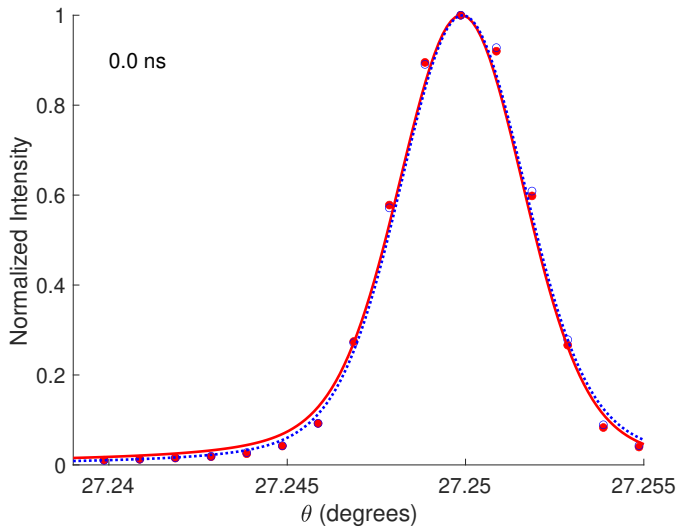

(a)

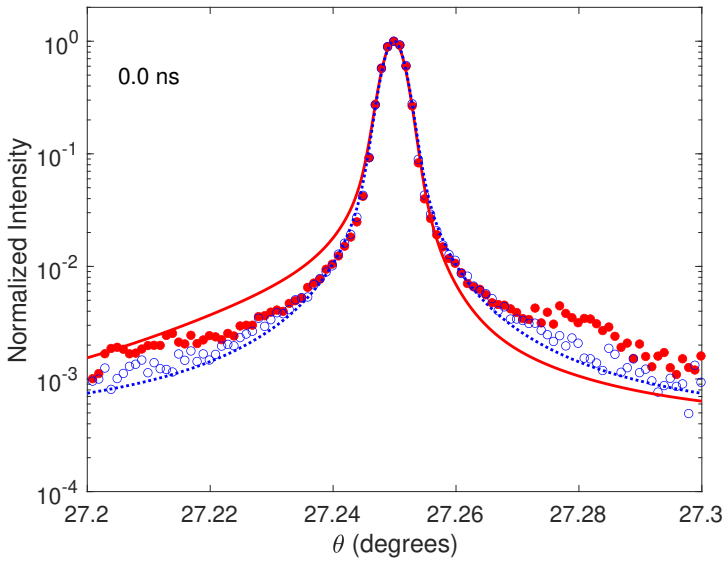

(b)

Figure 4.3: $t = 0$ ns diffraction data (red filled circles), classical thermal transport simulation (red line), and $t < 0$ data (open blue circles) and simulation (blue line). $t = 0$ ns or "time zero" is the earliest data point where a significant difference is seen in the x-ray data from the proceeding x-ray bunch.

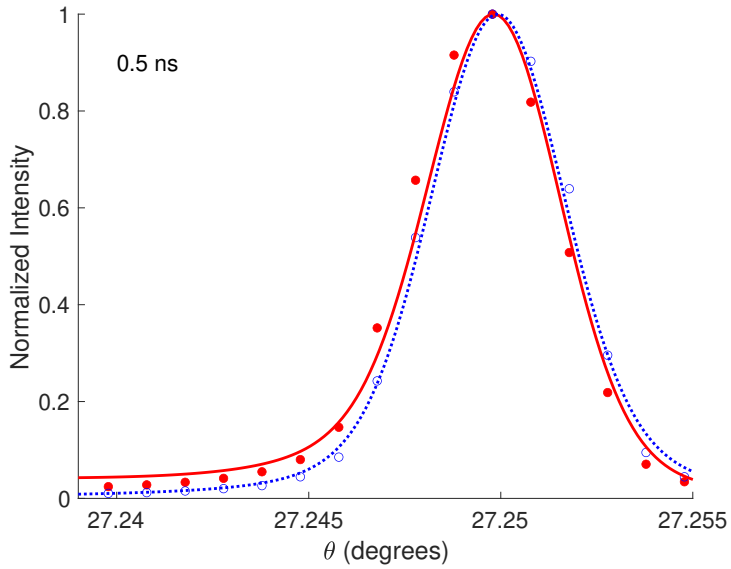

(a)

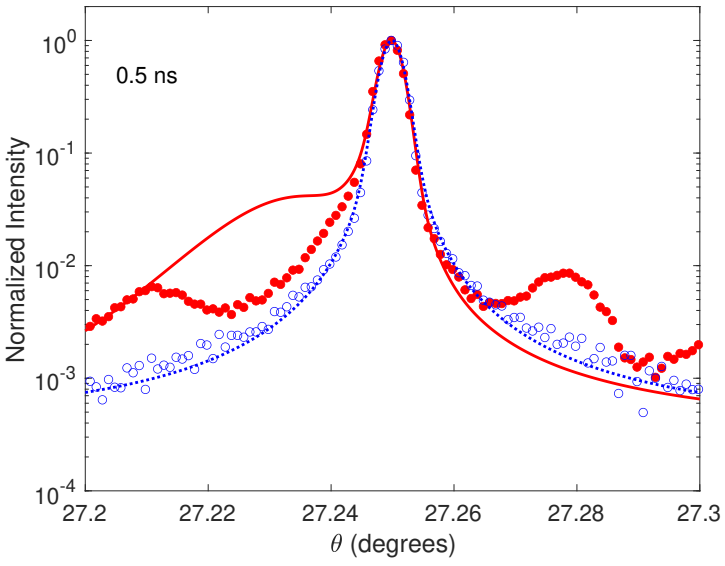

(b)

Figure 4.4: $t = 0.5$ ns diffraction data (red filled circles), classical thermal transport simulation (red line), and $t < 0$ data (open blue circles) and simulation (blue line). The x-ray data (which is entirely dependent upon the substrate) shows significant fringes which cannot be explained by the Fourier Law.

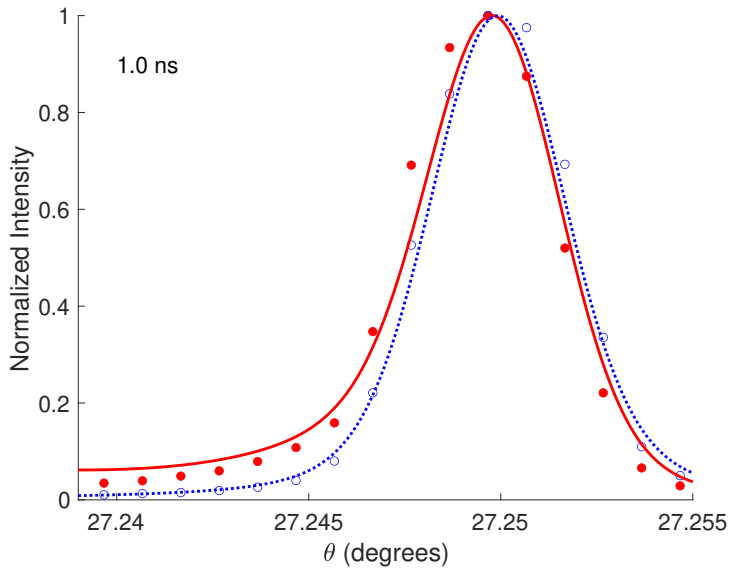

(a)

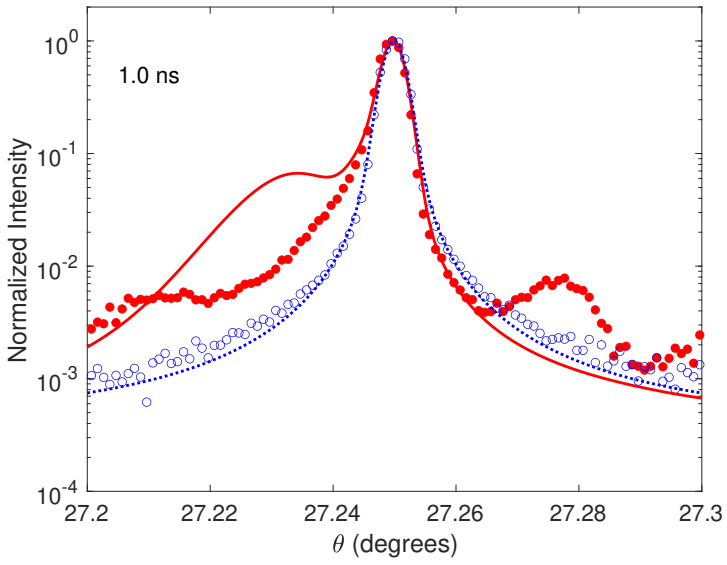

(b)

Figure 4.5: $t = 1.0$ ns diffraction data (red filled circles), classical thermal transport simulation (red line), and $t < 0$ data (open blue circles) and simulation (blue line). Both simulation and data peaks show a shifting and broadening, consistent with a non-uniform temperature gradient as the heat is just beginning to flow into the substrate. The Fourier Law simulation shows a greater average temperature than the data.

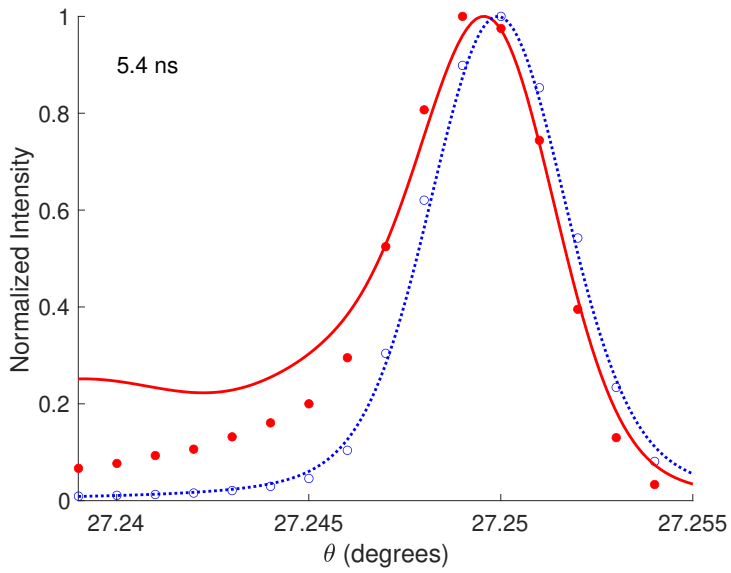

(a)

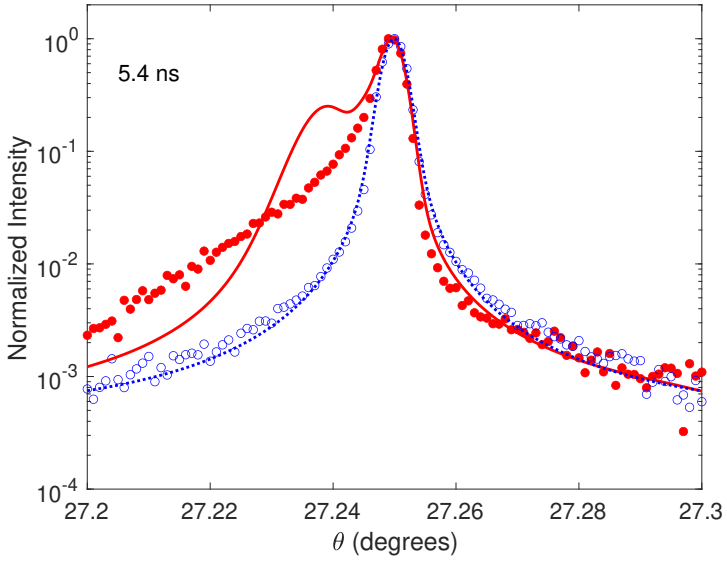

(b)

Figure 4.6: $t = 5.4$ ns diffraction data (red filled circles), classical thermal transport simulation (red line), and $t < 0$ data (open blue circles) and simulation (blue line). This is near the maximum centroid shift predicted by the Fourier simulation.

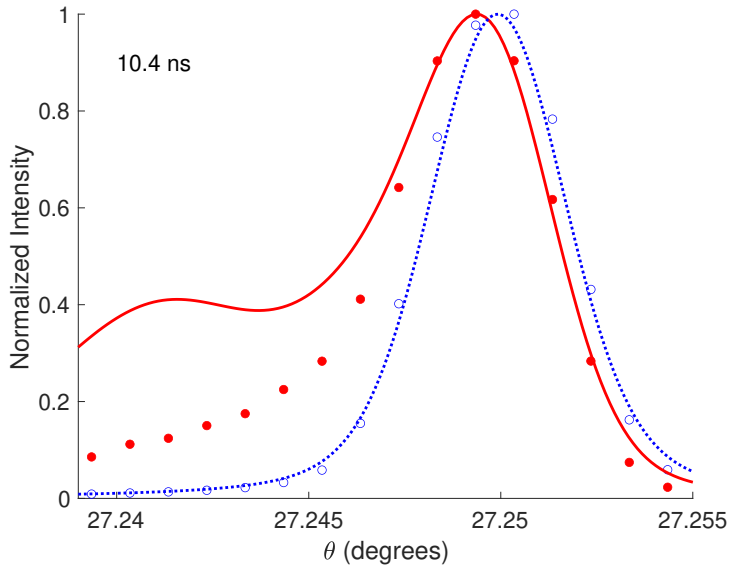

(a)

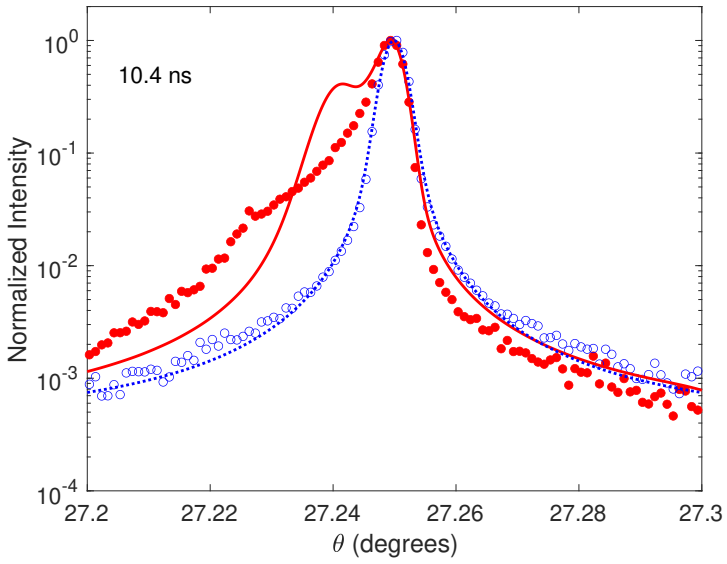

(b)

Figure 4.7: $t = 10.4$ ns diffraction data (red filled circles), classical thermal transport simulation (red line), and $t < 0$ data (open blue circles) and simulation (blue line). This is near the maximum centroid shift measured, but after the maximum shift found in the simulation.

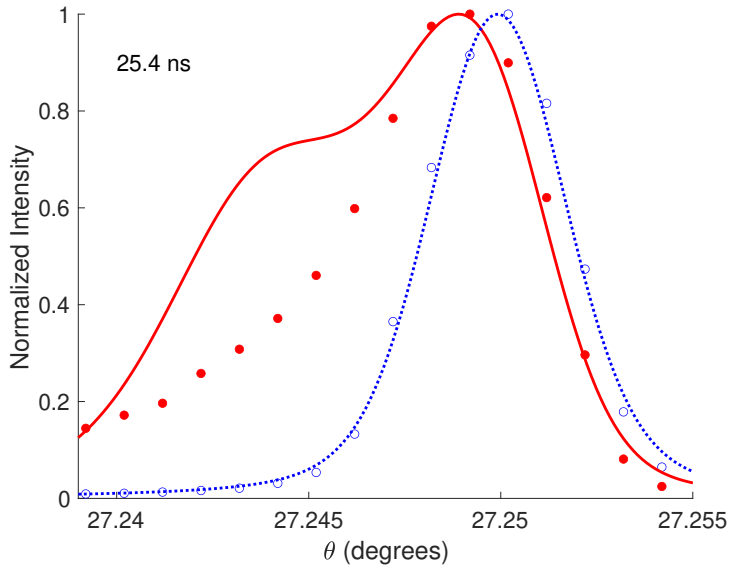

(a)

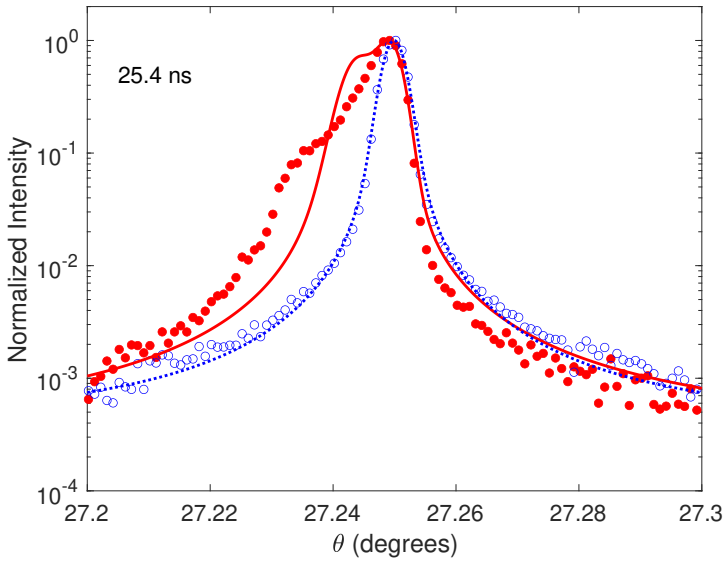

(b)

Figure 4.8: $t = 25.4$ ns diffraction data (red filled circles), classical thermal transport simulation (red line), and $t < 0$ data (open blue circles) and simulation (blue line). This is past the point of maximum peak shift for both the simulation and measurement, and just as cooling is starting.

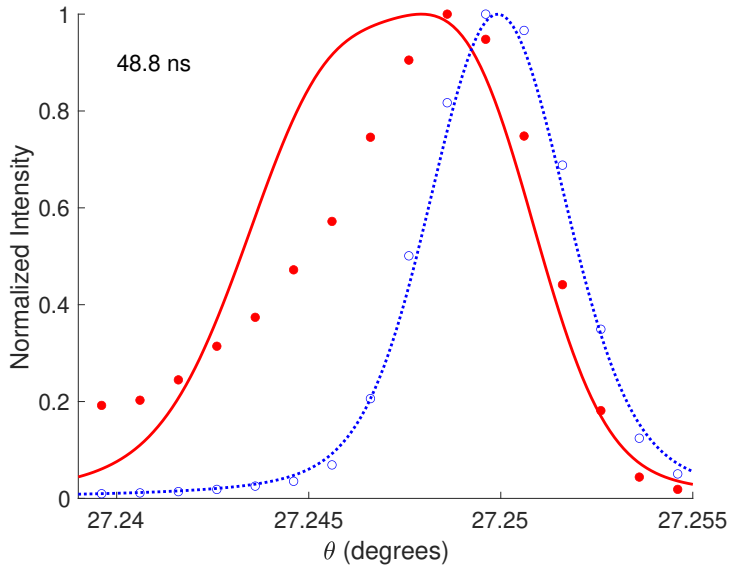

(a)

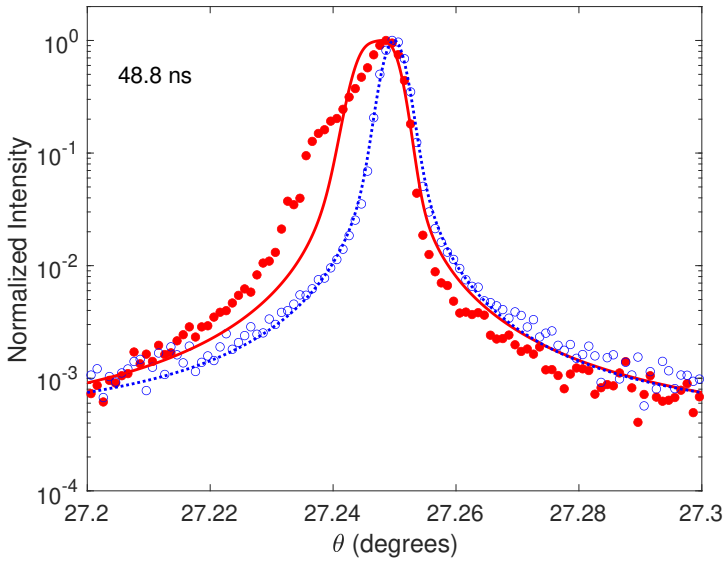

(b)

Figure 4.9: $t = 48.8$ ns diffraction data (red filled circles), classical thermal transport simulation (red line), and $t < 0$ data (open blue circles) and simulation (blue line). The calculated and measured peaks are beginning to narrow, indicating that temperature is becoming more homogenous throughout the substrate surface.

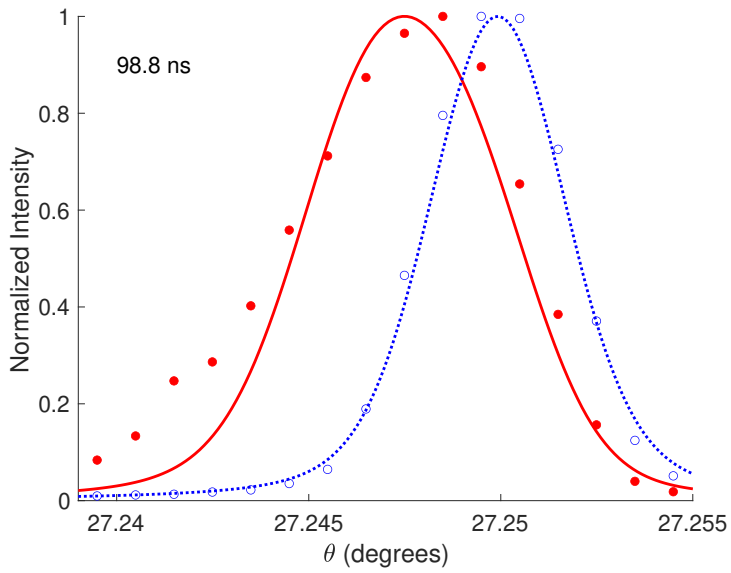

(a)

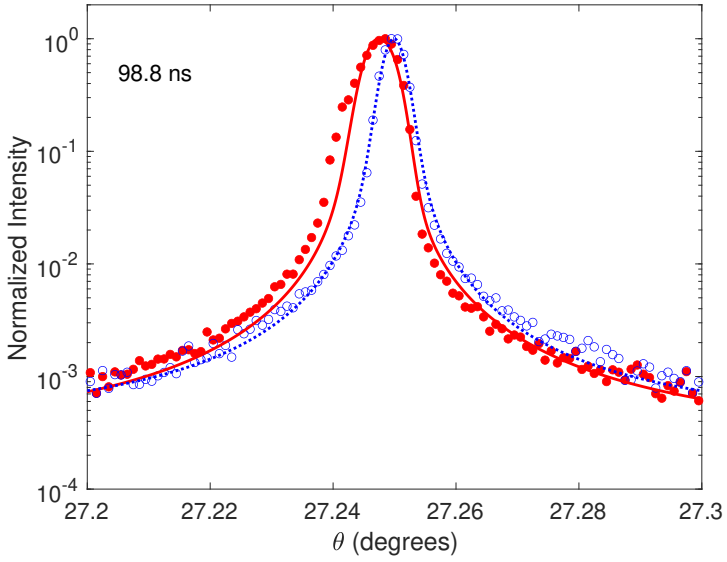

(b)

Figure 4.10: $t = 98.8$ ns diffraction data (red filled circles), classical thermal transport simulation (red line), and $t < 0$ data (open blue circles) and simulation (blue line). Cooling continues as the centroid shift reduces.

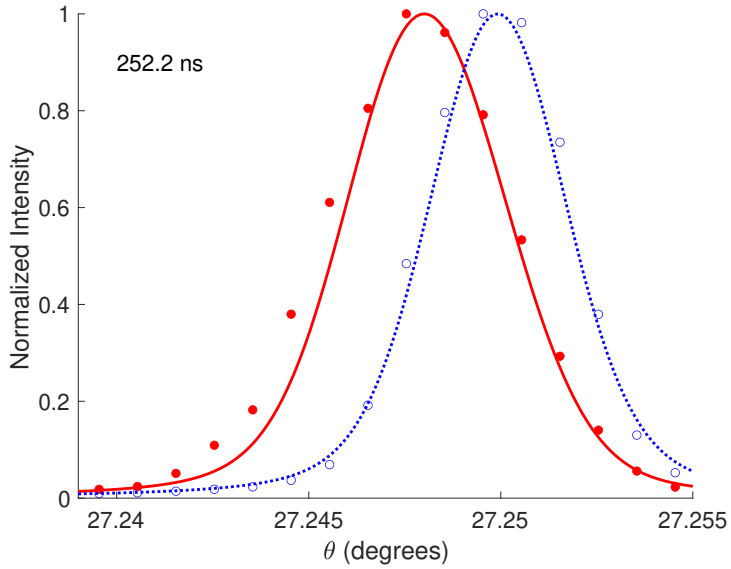

(a)

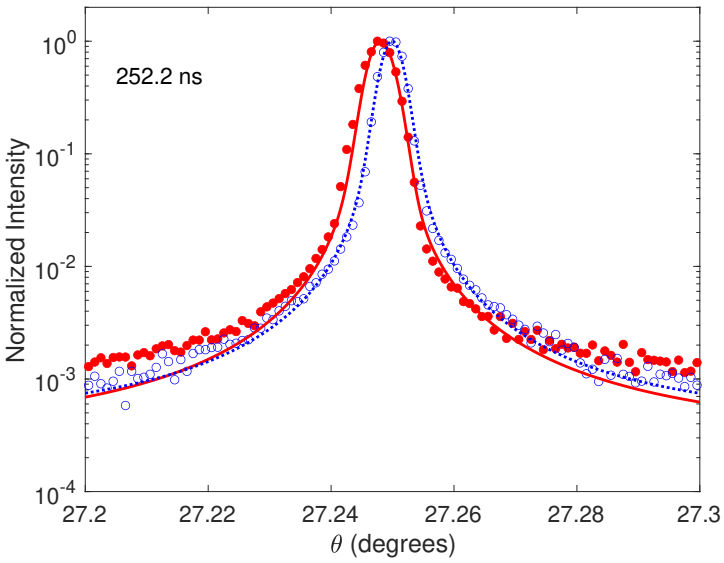

(b)

Figure 4.11: $t = 252.2$ ns diffraction data (red filled circles), classical thermal transport simulation (red line), and $t < 0$ data (open blue circles) and simulation (blue line). The strained and unstrained rocking curves now have similar shapes and widths, indicating that the probed length the substrate is at a uniform, but still elevated temperature.

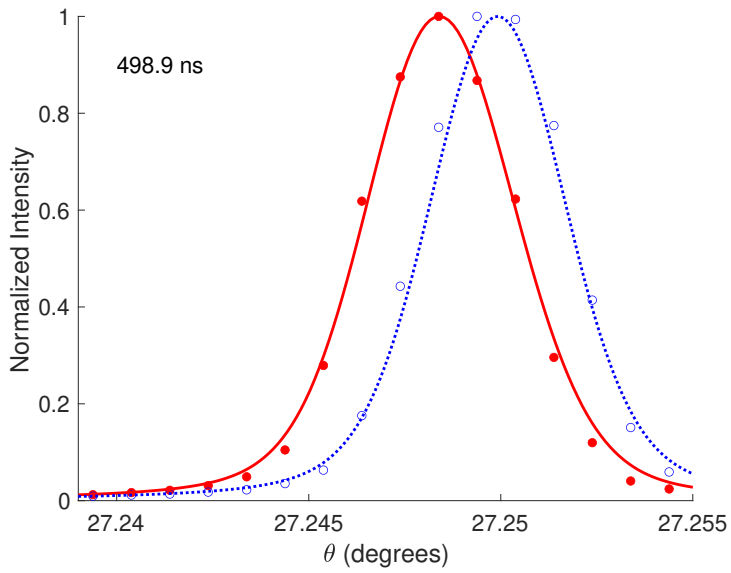

(a)

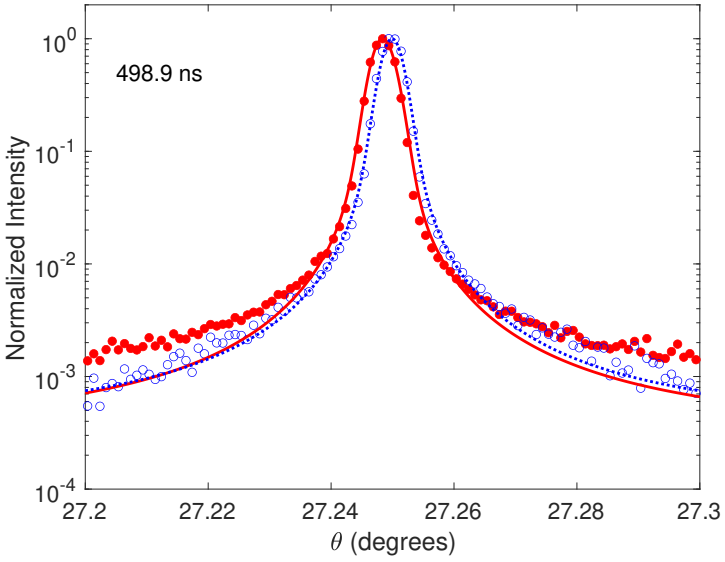

(b)

Figure 4.12: $t = 498.9$ ns diffraction data (red filled circles), classical thermal transport simulation (red line), and $t < 0$ data (open blue circles) and simulation (blue line). Agreement between the Fourier theory and measurement is now very close.

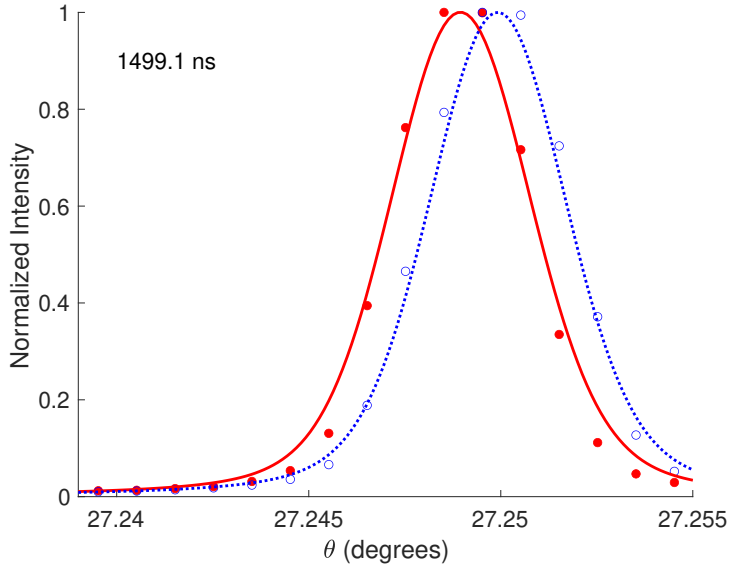

(a)

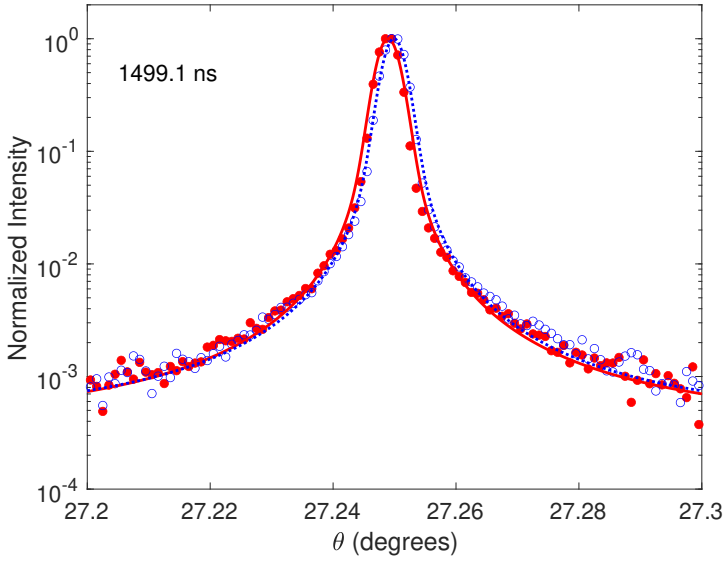

(b)

Figure 4.13: $t = 1499.1$ ns diffraction data (red filled circles), classical thermal transport simulation (red line), and $t < 0$ data (open blue circles) and simulation (blue line). The temperature difference is now a uniform 5 degrees C.

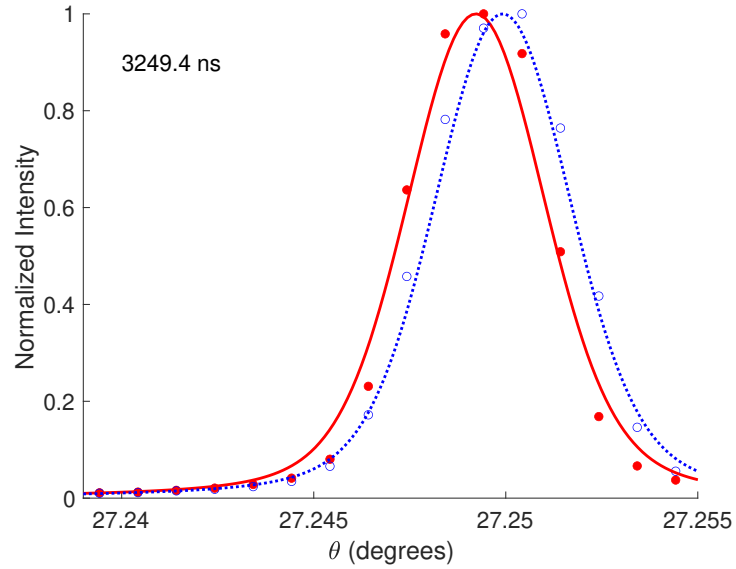

(a)

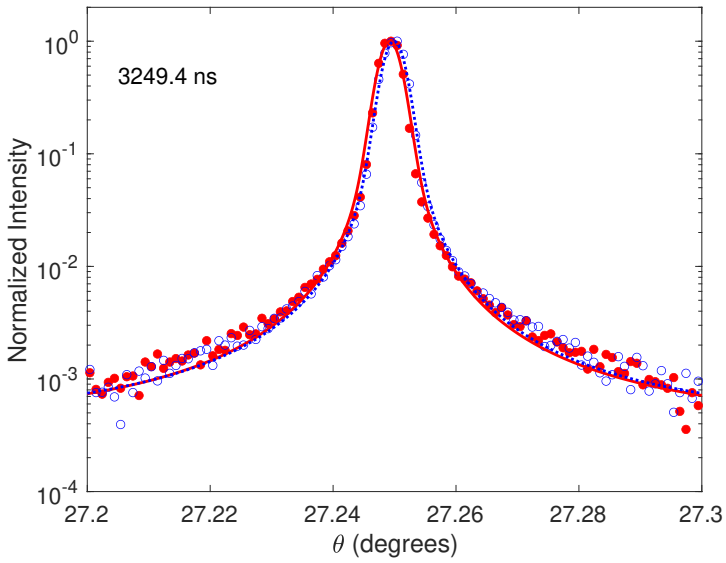

(b)

Figure 4.14: $t = 3249.4$ ns diffraction data (red filled circles), classical thermal transport simulation (red line), and $t < 0$ data (open blue circles) and simulation (blue line). By the latest timepoints recorded, the agreement between the Fourier Theory and measurement is almost as good as for the unstrained rocking curves. The strain is completely uniform throughout the probed crystal depth.

probing an extinction depth of over 2000 nm, meaning that only one fifth of probed volume is strained. Therefore, the Fourier Law would predict a strong double-peaked curve, corresponding two a thin strained layer near the surface and then the larger underlying bulk volume which remains unaffected at these times. When these early strain profiles are converted into diffraction peak shapes by $TRXD$, they do indeed show a double-peak which slowly merges with the main peak as time continues. By 25 ns, the Fourier Law predicts a single, significantly broadened peak as the strain continuously decreases all the way out to the x-ray extinction depth of 1.7 μm. This is seen in the simulation curves of Figs. 4.4 - 4.8.

However, the actual measured diffraction peaks completely disagree with calculation, indicating the the Fourier Law does not properly predict the shape of the temperature profile at $t < 25$ ns. Instead, the data initially shows symmetric fringes, implying both an expansion and a compression of GaAs. This previously undiscovered behavior is discussed in the next chapter. Given the disagreement about diffraction peak shape, it is no surprise that the calculated centroid peak shifts and average temperature of the GaAs as seen in Fig. 4.1 also disagrees with measurement at these times.

Once the heat impulse has travelled throughout the probe depth, we see that the Fourier Law begins to behave more qualitatively like the observations. The merged, broadened peak begins to narrow beginning at 100 ns (Fig. 4.10) as the strain profiles become uniform over the entire probed volume. By 1500 ns the laser-excited crystal has the same diffraction peak width as the initially unstrained crystal (Fig. 4.13, indicating a uniform but elevated tempearture that is also in quantitative agreement with the Fourier Law prediction. The experiment is now well within the regime of Fourier Law validity, as cooling of the probed volume continues via classical thermal diffusion as the heat flows into the unmeasured crystal bulk (Fig. 4.14. The crystal wafer is 500 μm thick, implying that it would take over 1 ms for heat to reach the rear side of the wafer. By this time, the next pulse of the 1 kHz repetition rate laser has hit the front surface with the metallic film, repeating the experiment.

CHAPTER 5

Discussion, summary, and outlook

5.1 New information on nanoscale thermal transport

The observation of modulations (indicating hot spots) at early timescales in the diffraction patterns (e.g. Fig. 4.4) is unexpected. A surface plot of the early dynamics is shown in Fig. 5.1, and it shows that the feature appears quickly and then decays. This is contrary to our expectation of the feature continuing to propagate at the speed of sound in GaAs (the anticipated speed of "ballistic phonons"). I suggest that these are nanoscale hotspots, and that they may be the failure mechanism of some nanoscale electronic devices. Importantly, they would not have been noticed in the previous x-ray study of nanoscale thermal transport [11], which only examined a single point on the diffraction peak rocking curve and interpreted data only using kinematic diffraction theory. Engineering around these inherent and transient "defects" in otherwise "perfect" crystal due to fundamental phonon behaviors will require a better understanding of their properties, which the techniques developed in this thesis can provide.

5.2 Thesis summary

In this document, we have benchmarked a new code specifically written for time-resolved studies, *TRXD*, against an existing tool for performing x-ray dynamical diffraction on strained crystals, *GID_SL*. We have then proceeded to validate TRXD against experimental lineshapes for a 100 nm GaAs bulk by convolving our TRXD results with voigt function. We found that the discrepancies between our experi-

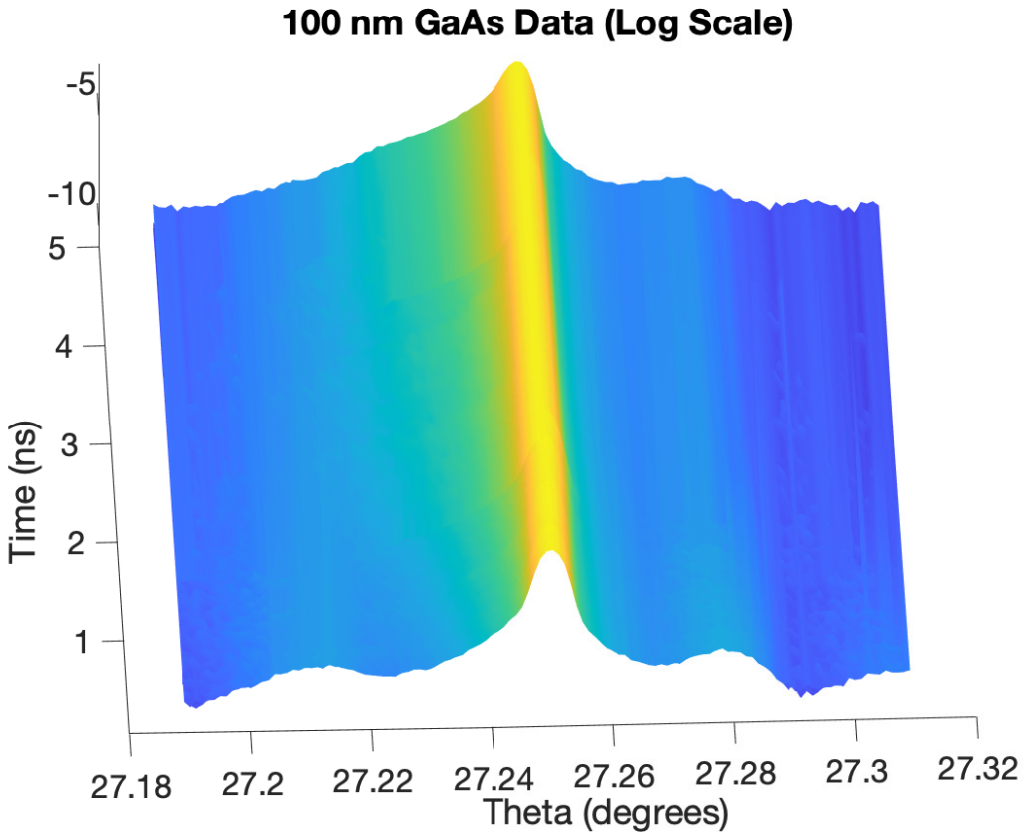

Figure 5.1: X-ray diffraction data showing the transient appearance of fringes which are stationary, but decay slowly in the first few nanosecond after laser excitation. This provides experimental evidence for non-uniform, non-propagating temperature distributions within semiconductor substrate.

mental results and Fourier Theory matched those of earlier work, suggesting heat transfers slower at short times and distances. Additionally, the data set we used contains the first structural data showing the appearance of non-uniform strain in a previously uniform crystal due to nanoscale thermal transport.

5.3 Outlook

Going forward, there are several ways this research can be improved or expanded upon. First, the data set used contains experimental data for lineshapes other than our 100 nm GaAs bulk with chromium film - TRXD should be tested against this additional data. This includes 100 nm, 200 nm, and 400 nm Cr films on not just GaAs, but also the bulk semiconductor materials InSb, Ge, and Si. Next, general methods for inverting dynamical diffraction data to calculate strain profiles (and therefore temperature profiles) should be implemented using *TRXD*, e.g. [16] and [17]. Additionally, the most recent theoretical models for nanoscale thermal transport, e.g. Lattice Boltzmann Models [2], should be tested against these new validated data sets and diffraction calculations. Finally, we will seek to determine the exact temperature depth profile and extract the phonon mean free path spectra directly from structure.

APPENDIX A

MATLAB codes

Below we will include the MATLAB code used to calculate the lineshape broadening and thermal film modeling presented in this thesis. The full set of codes for *TRXD* are available at [24].

```
% TRXD.m
% Program to calculate Time-Resolved X-Ray Diffraction
% By Eric Landahl, DePaul University Physics Department, ...
    elandahl@depaul.edu
% First written December 13, 2016
% Revised by EL 1.9.2017 to add unstrained amplitude output
% Revised by EL 1.16.17 to handle benchmarking to Sergey's GID
% Improved accuracy by fixing Δ and final step interpolation ...
    1/19/2017
% Corrected signs on p_0i, p_0r, p_Hi, p_Hr to work with X0h ...
    database 1/20/17
% Based on previous work by Sooheyong Lee (KRISS) and G. Jackson ...
    Williams (LLNL)
% Revised by JG 7.25.20 - added new inputs for thermalfilm.m to ...
    work.
% num_times MUST be set to 50 - code will not work otherwise
%
% INPUTS:
%   model           strain model, selected from the following list:
%     thermalFilm   Gaussian solution to prompt surface ...
    temperature rise
%   crystal         determines x-ray and strain properties, ...
    chosen from:
%     GaAs
```

```
18 %     Si
19 %     Ge
20 %     InSb
21 %   reflection  diffraction vector [h k l], i.e. [hkl] chosen from:
22 %     [0 0 4]
23 %   cut         surface normal vector [h k l], i.e. (hkl) chosen ...
       from:
24 %     [0 0 1]
25 %   energy      x-ray energy in keV
26 %   fluence     absorbed laser fluence in mJ/cm^2
27 %   angle       in degrees, one of the following:
28 %     a vector  angles to be calculated, relative to the Bragg angle
29 %     a value   a total range of angles, from which a vector is ...
       generated
30 %     0         a default is used
31 %   time        in seconds, one of the following:
32 %     a vector  times to be calculated, relative to time-zero
33 %     a value   a final time, from which a vector of times is ...
       generated
34 %     0         a default is used, based on the model
35 %   L           thickness of the film
36 %
37 % OUTPUTS:
38 %   A           X-ray scattering amplitude array, returned as ...
       A(time, angle)
39 %   A0          unstrained crystal scattering amplitude
40 %   time        a vector of times
41 %   angle       a vector of angles calculated, absolute, in degrees
42 %
43 % SAMPLE Usage:
44 % [A A0 time angle Strain z] = TRXD ('thermalFilm', 'Al', 'Si', ...
       [0 0 4], [0 0 1], 10, 1, 0, 0, 2e-7)
45
46
47 function [A A0 time angle Strain_save z] = TRXD (model, film, ...
       crystal, reflection, cut, energy, fluence, angle, time, L)
```

```
48 more off; % Turn on scrolling
49
50 %% Include subdirectories in path
51 addpath('main','include','strain_functions','data');
52
53 %% Some constants that can be changed to speed things up when ...
       using defaults
54 num_times = 103;
55 num_angles = 400;
56 time_f = 2.5e-9; % in seconds
57 angle_width = 2e-2; % in degrees
58
59 %% Check inputs
60
61 if nargin ~= 10
62   fprintf('Incorrect number of input arguments\n')
63   nargin
64   return
65 end
66
67 if (energy < 7) | (energy > 14)
68   fprintf('Energy out of range\n')
69   energy
70   return
71 end
72
73 if reflection ~= [0 0 4]
74   fprintf('Only [0 0 4] reflection is supported now.\n')
75   reflection
76 end
77
78 if cut ~= [0 0 1]
79   fprintf('Only [0 0 1] surface cut is supported now.\n')
80   cut
81   return
82 end
```

```
83
84  % Determine diffraction parameters
85
86  % Calculate assymetry angle; should be zero
87  phi = acos(dot(reflection/norm(reflection),cut/norm(cut)));
88  if phi > 1e-6
89    fprintf ('The assymetry angle is not zero.\n')
90    phi
91    return
92  end
93
94  % Load X0h data
95  if strcmp(crystal,'GaAs')
96    X0h = load ('GaAs400.dat');
97    ID = 1; % ID number for crystal data
98  elseif strcmp(crystal,'InSb')
99    X0h = load ('InSb400.dat');
100   ID = 2;
101 elseif strcmp(crystal,'Si')
102   X0h = load ('Si400.dat');
103   ID = 3;
104 elseif strcmp(crystal,'Ge')
105   X0h = load ('Ge400.dat');
106   ID = 4;
107 else
108   fprintf('Crystal needs to be either Si, GaAs, Ge, or InSb.\n')
109   crystal
110   return
111 end
112
113 % Interpolate X0h data
114 % Note that X0h(:,1) are the energies in keV
115 p_0r = -abs(interp1(X0h(:,1), X0h(:,2), energy, 'spline', ...
        'extrap'));
116 p_0i = abs(interp1(X0h(:,1), X0h(:,3), energy, 'spline', 'extrap'));
117 p_Hr = -abs(interp1(X0h(:,1), X0h(:,4), energy, 'spline', ...
```

```
    'extrap'));
p_Hi = abs(interp1(X0h(:,1), X0h(:,5), energy, 'spline', 'extrap'));
Δ = interp1(X0h(:,1), X0h(:,6), energy, 'spline', 'extrap');
tB_deg = interp1(X0h(:,1), X0h(:,7), energy, 'spline', 'extrap');
thetaB= tB_deg*pi/180;  % Sergey Si, Bragg angle in radians
lambda= energy*1.23984193E-11; % convert energy in keV to ...
    wavelength in meters

% Assemble params arrray containing parameters for the crystal ...
    diffraction
params(1) = p_0r + 1i*p_0i;
params(2) = p_Hr + 1i*p_Hi;
params(3) = thetaB;
params(4) = phi;
params(5) = Δ;
params(6) = lambda;

% Assemble opts array containing options for adaptative depth ...
    stepping
tol = 1e-4; % tolerance.  Higher value for more speed and less ...
    precision
dz_min = 1e-10; % Minimum step size in meters
dz_max = 1.1e-8; % Maximum step size in meters
f = 5; %Shift factor for convergence

opts(1) = tol;
opts(2) = dz_min;
opts(3) = dz_max;
opts(4) = f;

% Calculate extinction length
gamma0 = sin(thetaB+phi);
gammaH = sin(thetaB-phi);
Lext = lambda*sqrt(abs(gammaH)*gamma0)/(pi*abs(p_Hr));

%% Calculate time array
```

```
149 if time == 0
150   time = time_f; % set default maximum time delay to default
151 end
152 if (length(time)==1)
153   dt =time; % save for external file function
154   time = time/num_times:time/num_times:time;
155 end
156
157 %% Calculate angular array
158 if (angle == 0)
159   angle = angle_width; % set default angular width to 10 mdeg
160 end
161 if (length(angle)==1)
162   angle = (0:angle/num_angles:angle)-0.9*angle/2;
163 end
164
165 angle = thetaB + angle*pi/180; % Convert angle to radians and ...
      add Bragg Angle
166
167 if strcmp(model,'thermalFilm')
168   [longitudinal trans sheer time_out z] = thermalFilm (film, ...
        crystal, fluence, time, 5.1*Lext, L);
169 elseif strcmp(model,'strainFile')
170   z = load('depth_file.txt');
171   time_out = load('time_file.txt');
172   longitudinal = load('strain_file.txt');
173   trans = 0*longitudinal;
174   sheer = 0*longitudinal;
175 elseif strcmp(model,'strainFile1D') % strains just at one time
176   z = load('depth_file.txt');
177   time_file = load('time_file.txt');
178   time_out = time_file(fluence); % No time specified, just ...
        strain at one time
179   all_strain = load('strain_file.txt');
180   longitudinal = all_strain(floor(fluence),:); % load only one ...
        column
```

```
181    trans = 0*longitudinal;
182    sheer = 0*longitudinal;
183    time=time_out;
184  elseif strcmp(model,'benchmark')
185    clear time;
186    time = 1;
187    time_out = 1;
188    dz = 5.1*Lext/10000; % 10,000 depth points out to 5.1*Lext
189    z = dz*(1:10000);
190    trans = 0.*z; % no transverse strain
191    sheer = 0.*z; % no sheer strain
192    %longitudinal = 0.*z;
193    longitudinal = 1e-4 * (z<=2e-6); % Simple strain model
194  else
195    fprintf('Not a valid model\n')
196    return
197  end
198
199   % Need to add a single timepoint test for comparisson with ...
         Sergey's GID
200   % Otherwise seems to work 12/28/16 EL
201
202  for m = 1: length(time)
203    fprintf('Evaluating rocking curve at %e s.\n',time_out(m))
204    if time(m) == time_out(m) % if the time doesn't need to be ...
         remeshed
205      st1(m,:) = longitudinal(m,:);
206      st2(m,:) = trans(m,:);
207      st3(m,:) = sheer(m,:);
208    else % remesh time if necessary
209      st1(m,:) = interp1(time_out,longitudinal,time(m), 'spline', ...
           'extrap');
210      st2(m,:) = interp1(time_out,trans,time(m), 'spline', 'extrap');
211      st3(m,:) = interp1(time_out,sheer,time(m), 'spline', 'extrap');
212    end
213    Strain_in = [st1(m,:)' st2(m,:)' st3(m,:)']; % Evaluate strain ...
```

```
        at each time
214   [X X0 err Steps Strain_out] = WieAdapt (Strain_in, z, angle, ...
        opts, params);
215   A0 = X0.*conj(X0); % Unstrained crystal intensity
216   A(m,:) = X.*conj(X); % Intensity Amplitude
217   Strain_save(m,:,:) = Strain_out(:,:);
218 %   x = 1:10000;
219 %   strainsave = sprintf('strain%d.png',m);
220 %
221 %   figure
222 %   plot(x, Strain_out(:,:))
223 %   saveas(gcf,strainsave)
224 end
225
226 if strcmp(model,'benchmark')
227   % Keep angle in absolute radians
228   angle = (angle)*180/pi; % Convert angle back to degrees ...
        relative to Bragg
229 else
230   angle = (angle)*180/pi; % Convert angle back to degrees ...
        relative to Bragg
231 end
232
233 figure
234 plot(angle,A)
235 xlabel('Angle')
236 ylabel('Intensity')
237
238 % rang1 = (-60:0.3:60);
239 % rang2 = (-60:0.2308:60.2308);
240 % rang3 = (-60:1:60);
241 %
242 % phi = rang1 * (pi/360);
243 %
244 % res = exp( -(phi.^2)/(den));
245 %
```

```
% convol = conv(A,res);
%
% plot(rang3,rocking/max(rocking))
% hold on
% plot(rang2,convol)
% xlabel('Angle')
% ylabel('Normalized Intensity')
% legend('Experimental','Theoretical')


% T = [angle; A0];
%
% fileID = fopen('tabledata.txt','w');
% fprintf(fileID,'%6s %12s\n','angle','intensity');
% fprintf(fileID,'%6.2f %12.8f\n',T);
% fclose(fileID);

%hold on

%plot(Output.Angle,Output.Intensity)
```

```
%This script will run a loop comparing the theoretical and ...
    experimental
%rocking curves obtained from TRXD.
%
%
%
%
%Variables
%   n         The number of iterations we want to run the script for
%   RoCur     The experimental rocking curve data we are ...
    interested in
%   control   The TRXD results for the data we are interested in
%   Ang       The angles for our experimental rocking curve data
%   std       The denominator for the exponential in the gaussian
```

```
13 %   Time      The time table for our experimental rocking curve data
14 %   a         The asymmetry factor for the asymmetrical lorentzian
15
16 function TRXDloop(n,RoCur,Ang,std,a,model, film, crystal, ...
       reflection, cut, energy, fluence, angle, time, L, ...
       gaussianwidth, lorentzianwidth, offset)
17     %run TRXD
18     [A A0 time angle Strain_save z] = TRXD (model, film, ...
           crystal, reflection, cut, energy, fluence, angle, time, L);
19
20     %surfacedata = [];
21
22     %this for loop allows the comparison function to be run as ...
           many times
23     %as needed without having to manually change inputs multiple ...
           times
24
25
26     for c = 1:n
27         %create the save names for the plots
28         svnmlin = sprintf('lintimestamp%d.png',c);
29         svnmlog = sprintf('logtimestamp%d.png',c);
30
31         %the comparison function
32         [convol] = ...
               comparison(RoCur(:,c),A(c,:),std,svnmlin,svnmlog,Ang(1,c),Ang(121,c),A
33
34         %surfacedata(n,:) = convol;
35
36     end
37
38     %figure
39     %surf(surfacedata,'edgecolor','none')
40
41 end
42
```

```
43
44 function [convol] = ...
       comparison(rocur,control,den,linname,logname,rangb,range,ang,time,a)
45
46 %convert sample data tables to arrays
47 beginning = table2array(rangb);
48 finish = table2array(range);
49 rocking = table2array(rocur);
50 angles = table2array(ang);
51
52
53
54 %create ranges based off of angles for the sample. rang is for ...
       plotting
55 %the resolution function, rangconvol is for plotting the convolution
56 rang = (beginning:0.3:finish);
57 rangconvol = (beginning:0.15:finish);
58
59 %convert range of angles to radians
60 phi = rang * (pi/180);
61
62 %laser resolution function
63 %res = exp( -(phi.^2)/(den));
64 % gamma = (2*60)./(1 + exp(a*phi));
65 % res = (2./(pi*gamma))./(1 + 4*(phi./gamma).^2);
66
67
68
69 %convolve theoretical rocking curve with function used to test laser
70 %resolution
71 convol = conv(control,res);
72
73
74
75 %for troubleshooting - most common error so far seems to be ...
       lengths not
```

```
%matching

% convol/max(convol)
% res/max(res)
% control/max(control)

% length(rangconvol)
% length(convol)
% length(res)

% length(rocking)
% length(angles)

%create and save linear figure comparing theoretical and ...
    experimental
%rocking curves

% figure
% plot(rang,res)

figure
plot(angles,rocking/max(rocking))
hold on
plot((rangconvol-5.55),convol/max(convol))
%xlim([-5 5])
xlabel('Angle')
ylabel('Normalized Intensity')
legend('Experimental','Theoretical')
title(['Timestamp ', num2str(time), ' seconds'])
saveas(gcf,linname)

%create and save logarithmic figure comparing theoretical and ...
    experimental
%rocking curves
figure
semilogy(angles,rocking/max(rocking))
```

```
110 hold on
111 semilogy((rangconvol-5.55),convol/max(convol))
112 %xlim([-5 5])
113 ylim([1e-3 1])
114 xlabel('Angle')
115 ylabel('Normalized Intensity')
116 legend('Experimental','Theoretical')
117 title(['Timestamp ', num2str(time), ' seconds'])
118 saveas(gcf,logname)
119
120 end
```

```
1  function [temperature strain] = shift2temp(thetaShift, ...
       thetaBragg, crystal);
2  % determine average temperature shift from average Bragg peak shift
3  % Eric Landahl, June 25, 2021
4  % INPUTS
5  %     thetaShift      Bragg angle shift IN DEGREES
6  %     thetaBragg      Bragg angle OM DEGREES
7  %     crystal         String of crystal abbreviation, e.g. 'Si'
8  % OUTPUT
9  %     temperature     Average temperature change in deg K
10 %     strain          unitless, Δ-d / d (d is lattice spacing)
11 % REQUIRES
12 %     sampledata
13 % EXAMPLE USAGE
14 %     [temperature strain] = shift2temp(-1e-3,27.24,'GaAs')
15 %         should return 5.9 deg K temperature increase, stain of ...
       3.4e-5
16 % OTHER USAGE
17 %     Calculate strain/temperature to check thermal expasion ...
       coef. alpha_t
18 %         ex: strain/temperature = 5.73e-6 1/K for example above
19
20 % Convert to radians
```

```
    thetaShift = thetaShift*pi/180;
    thetaBragg = thetaBragg*pi/180;

sampledata % load material properties
  ID = find(strcmp({sample.name}, crystal)==1);
  alpha_t = sample(ID).thermalExpansion.val; % 1/K

strain = - thetaShift * cot(thetaBragg);
temperature = strain/alpha_t;
```

```
%JimmyFigs.m
% Making extra figures for J. Grammich MS Thesis
% E. Landahl, 6-25-21
%
% REQUIRES
%    dataLoader.m must have already been run to save workspace ...
    of data and
%    simulations
%    shift2temp.m needed to calculate temperature shifts from ...
    angle shifts
%
clear all;
close all;
load('GaAs_100nm_data.mat'); % Load entire workspace

%% . OLD STUFF, IGNORE
% blur = 72;
% A = smoothdata(AA,2,'gaussian',blur); % Convolve with ...
    experimental angular resolution
% A0 = smoothdata(AA0,'gaussian',blur);

%theta0 = theta0 - 0.0005; % Account for shift between theory ...
    and data

clear A
```

```
clear A0

f = AA0;  % unstrained simulation result
gamma = 0.00035; % Cauchy width of instrument in degrees
sigma = 0.00145; % Gaussian width of instrument in degrees
g1 = (1/(sigma*sqrt(2*pi)))*exp(-0.5*(dtheta./sigma).^2); % Gaussian
g2 = (gamma/pi)./(dtheta.^2 + gamma^2); % Cauchy / Lorentzian
g = conv(g1,g2,'same'); % Voigt
g = g/max(g);
h = conv(f,g,'same'); % to compare to measurement
h = h + .005; % add offset
h = h/max(h);
g1 = (1/(sigma*sqrt(2*pi)))*exp(-0.5*(dtheta./sigma).^2); % Gaussian
g2 = (gamma/pi)./(dtheta.^2 + gamma^2); % Cauchy / Lorentzian
g = conv(g1,g2,'same'); % Voigt
g = g/max(g);
h = conv(f,g,'same'); % to compare to measurement
h = h + .005; % add offset
h = h/max(h);

A0 = h;

for j = 1: length(newTime)
    f = AA(j,:);
    g1 = (1/(sigma*sqrt(2*pi)))*exp(-0.5*(dtheta./sigma).^2); % ...
        Gaussian
    g2 = (gamma/pi)./(dtheta.^2 + gamma^2); % Cauchy / Lorentzian
    g = conv(g1,g2,'same'); % Voigt
    g = g/max(g);
    h = conv(f,g,'same'); % to compare to measurement
    h = h + .005; % add offset
    h = h/max(h);
    A(j,:) = h;
end

%theta0 = theta0-.0005;
```

```
57
58 %% Centroid shifts from calculations
59 center0 = centroid(dtheta,A0);  %A0 is calculated unstrained ...
       rocking curve
60 for i = 1:length(newTime)
61     centerShiftCalc(i) = 1000*(centroid(dtheta,A(i,:))-center0);
62 end
63
64 %% This figure just shows the calculation results
65 figure(3);clf;hold on
66      plot(newTime,centerShiftCalc,'-')
67     xlabel('Time (ns)')
68     ylabel('Cetroid Shift Calculated (mdeg)')
69     %title('GaAs with 100 nm Cr coating')
70     legend(gca,'off')
71     ax = gca;
72     ax.FontSize = 16;
73 hold off;
74
75 %% Add calcs to linear centroid shift plot
76 % figure(1);hold on
77 %     plot(newTime,centerShiftCalc,'.r','LineWidth',2)
78 %     saveas(1,['~/Documents/Jimmy/figures/LinSim+Data.png'])
79 %     saveas(1,['~/Documents/Jimmy/figures/LinSim+Data.fig'])
80 %     saveas(1,['~/Documents/Jimmy/figures/LinSim+Data.eps'])
81 % hold off
82 %
83 % %% Add calcs to log centroid shift plot
84 % figure(2);hold on
85 %     semilogx(newTime,centerShiftCalc,'.r','LineWidth',2)
86 %     saveas(2,['~/Documents/Jimmy/figures/LogSim+Data.png'])
87 %     saveas(2,['~/Documents/Jimmy/figures/LogSim+Data.fig'])
88 %     saveas(2,['~/Documents/Jimmy/figures/LogSim+Data.eps'])
89 % hold off
90
91 %% Simulation surface plots
```

```
92 figure(6);clf; hold on;
93     surf(dtheta+theta0,newTime,A);
94     shading interp;
95     ylim([0 max(timePos)]);
96     xlim([27.239 27.255])
97     xlabel('Theta (degrees)')
98     ylabel('Time (ns)')
99     title('100 nm Cr film on GaAs Simulation')
100    ax = gca; ax.FontSize=16;
101    saveas(6,['¬/Documents/Jimmy/figures/LinSim.png'])
102    saveas(6,['¬/Documents/Jimmy/figures/LinSim.fig'])
103    saveas(6,['¬/Documents/Jimmy/figures/LinSim.eps'])
104 hold off
105
106 figure(7);clf; hold on;
107    surf(dtheta+theta0,newTime,log(A));
108     ylim([0.048 5]); shading interp;
109    xlabel('Theta (degrees)')
110    ylabel('Time (ns)')
111    title('100 nm GaAs Simulation (Log Scale)')
112    ax = gca; ax.FontSize=16;
113    saveas(7,['¬/Documents/Jimmy/figures/LogSim.png'])
114    saveas(7,['¬/Documents/Jimmy/figures/LogSim.fig'])
115    saveas(7,['¬/Documents/Jimmy/figures/LogSim.eps'])
116 hold off
117
118 %% Plots at particular timepoints
119 % Hint:   k = find(abs(timePos-5) < 0.05 to find index k near 5 ns
120
121 k0 = 1; %  Before time zero
122 timek0 = newTime(k0);
123 % figure(8);clf;hold on
124 %     plot(theta,On(k0,:)/max(On(k0,:)),'bo')
125 %     plot(dtheta+theta0,A0/max(A0),':b')
126 %     text(27.24,.9,[num2str(timek0,'%.1f') ' ns'],'FontSize',16)
127 %     xlabel('\theta (degrees)')
```

```
128 %     ylabel('Normalized Intensity')
129 %     xlim([27.239 27.255])
130 %     ax = gca; ax.FontSize=16;
131 %     saveas(8,['¬/Documents/Jimmy/figures/Unstrained_LinRock.png'])
132 %     saveas(8,['¬/Documents/Jimmy/figures/Unstrained_LinRock.eps'])
133 %     saveas(8,['¬/Documents/Jimmy/figures/Unstrained_LinRock.fig'])
134 % hold off;
135 % figure(9);clf;
136 %     semilogy(theta,On(k0,:)/max(On(k0,:)),'bo');hold on;
137 %     semilogy(dtheta+theta0,A0/max(A0),':b')
138 %     text(27.19,.5,[num2str(timek0,'%.1f') ' ns'],'FontSize',16)
139 %     xlabel('\theta (degrees)')
140 %     ylabel('Normalized Intensity')
141 %     ax = gca; ax.FontSize=16;
142 %     saveas(9,['¬/Documents/Jimmy/figures/Unstrained_LogRock.png'])
143 %     saveas(9,['¬/Documents/Jimmy/figures/Unstrained_LogRock.eps'])
144 %     saveas(9,['¬/Documents/Jimmy/figures/Unstrained_LogRock.fig'])
145 % hold off;
146
147 k05 = 10; % 0.5 ns;
148 k1 = 21; % 1 ns
149 k5 = 64; % 5 ns
150 k10 = 71; % 10 ns
151 k25 = 92; %25 ns
152 k50 = 104; % 50 ns
153 k100 = 124; % 100 ns
154 k250 = 163; % 250 ns
155 k500 = 209; % 500 ns
156 k750 = 258; % 750 ns
157 k1000 = 305; % 1 us
158 k1250 = 351; % 1.25 us
159 k1500 = 399; % 1.5 us
160 k1750 = 446; %1.75 us
161 k2000 = 493; % 2 us
162 k2250 = 541; % 2.25 us
163 k2500 = 588; % 2.5 us
```

```
164 k2750 = 636; % 2.75 us
165 k3000 = 683; % 3 us
166 k3250 = 729; % 3.25 us
167
168
169 k = [k0 k05 k1 k5 k10 k25 k50 k100 k250 k500 k750 k1000 k1250 ...
        k1500 k1750 k2000 k2250 k2500 k2750 k3000 k3250];
170 timek = newTime(k);
171 is = 118; % index shifter for data vs simulation
172 thetaBmp = -0.001;
173 for i = 1:length(k)
174     figure(7+i);clf;hold on;
175     plot(theta+theta0-thetaBmp-centerOff(k(i)+is),On(k(i)+is,:)/max(On(k(i)+is,:))
176     plot(theta+theta0-thetaBmp-centerOff(k(i)+is),Off(k(i)+is,:)/max(Off(k(i)+is,
177     plot(dtheta+theta0,A(k(i),:)/max(A(k(i),:)),'-r','LineWidth',2)
178     plot(dtheta+theta0,A0/max(A0),':b','LineWidth',2)
179     text(27.24,.9,[num2str(newTime(k(i)),'%.1f') ' ...
            ns'],'FontSize',16)
180     xlabel('\theta (degrees)')
181     ylabel('Normalized Intensity')
182     xlim([27.239 27.255]);
183     ax = gca; ax.FontSize=16;
184     saveas(7+i,['¬/Documents/Jimmy/figures/' ...
            num2str(timek(i),'%.1f') 'ns_''LinRock.png'])
185     saveas(7+i,['¬/Documents/Jimmy/figures/' ...
            num2str(timek(i),'%.1f') 'ns_''LinRock.eps'])
186     saveas(7+i,['¬/Documents/Jimmy/figures/' ...
            num2str(timek(i),'%.1f') 'ns_''LinRock.fig'])
187 end
188
189
190
191 for i = 1:length(k)
192     figure(29+i);clf;
193     semilogy(theta+theta0-thetaBmp-centerOff(k(i)+is),On(k(i)+is,:)/max(On(k(i)+is
            on;
```

```
194     semilogy(theta+theta0-thetaBmp-centerOff(k(i)+is),Off(k(i)+is,:)/max(Off(k(i)+
195     semilogy(dtheta+theta0,A(k(i),:)/max(A(k(i),:)),'-r','LineWidth',2)
196     semilogy(dtheta+theta0,A0/max(A0),':b','LineWidth',2)
197     text(27.205,.5,[num2str(newTime(k(i)),'%.1f') ' ...
            ns'],'FontSize',16)
198     xlabel('\theta (degrees)')
199     ylabel('Normalized Intensity')
200     xlim([27.2 27.3]);
201     ylim([1e-4 2]);
202     ax = gca; ax.FontSize=16;
203     saveas(29+i,['¬/Documents/Jimmy/figures/' ...
            num2str(timek(i),'%.1f') 'ns_''LogRock.png'])
204     saveas(29+i,['¬/Documents/Jimmy/figures/' ...
            num2str(timek(i),'%.1f') 'ns_''LogRock.eps'])
205     saveas(29+i,['¬/Documents/Jimmy/figures/' ...
            num2str(timek(i),'%.1f') 'ns_''LogRock.fig'])
206 end
207
208
209 %% Surface plots
210 figure(4);clf; hold on;
211     surf(theta,timePos,OnPos);
212     shading interp;
213     ylim([0 max(timePos)])
214     xlim([27.239 27.255])
215     xlabel('Theta (degrees)')
216     ylabel('Time (ns)')
217     title('100 nm Cr film on GaAs Data')
218     ax = gca; ax.FontSize=16;
219  hold off
220
221 figure(5);clf; hold on;
222     surf(theta,timePos,log(OnPos)); caxis([-11 -2.7]);
223     zlim([-11 -2.7]); ylim([0.048 5]); shading interp;
224     xlabel('Theta (degrees)')
225     ylabel('Time (ns)')
```

```
226     title('100 nm GaAs Data (Log Scale)')
227     ax = gca; ax.FontSize=16;
228  hold off
229
230
231 temperature = shift2temp(centerShift/1000, theta0, 'GaAs');
232
233 %% Linear Plot
234 figure(1); clf; hold on;
235     yyaxis left
236     h1 = plot(time,centerShift,'ro')
237     h2 = plot(newTime,centerShiftCalc,'-k','LineWidth',2)
238     xlabel('Time (ns)')
239     ylabel('Centroid shift (mdeg)')
240     yyaxis right
241     h3 =plot(time,temperature,'Marker','none','LineStyle','none')
242     ax = gca;
243     ax.YDir = 'reverse'
244     ylabel('Temperature shift (K)')
245     ax.YAxis(1).Color = 'k';
246     ax.YAxis(2).Color = 'k';
247     ax.FontSize = 16;
248
249     % Inset
250     bx = axes('Position',[.5 .2 .3 .3])
251     hold on;
252     plot(time,centerShift,'ro')
253     plot(newTime,centerShiftCalc,'-k','LineWidth',2)
254     xlim([-10 50]);
255     bx.FontSize = 16;
256     bx.TickLength = [0.02 0.02];
257     bx.LineWidth = 1;
258
259 hold off
260
261 %% Log Plot
```

```
figure(2); clf;
    yyaxis left
    h1 = semilogx(time,centerShift,'ro');
    hold on;
    h2 = semilogx(newTime,centerShiftCalc,'-k','LineWidth',2)
    xlabel('Time (ns)')
    ylabel('Centroid shift (mdeg)')
    yyaxis right
    h3 = ...
        semilogx(time,temperature,'Marker','none','LineStyle','none')
    ax = gca;
    ax.YDir = 'reverse'
    ylabel('Temperature shift (K)')
    ax.YAxis(1).Color = 'k';
    ax.YAxis(2).Color = 'k';
    ax.FontSize = 16;
hold off


%% Plots for trouble shooting (not saved)
%
% is = 119; % index shifter for data vs simulation
%
% for i = 1:length(newTime)
%     k(i)=i;
%     figure(200);clf;hold on;
%     ...
    plot(theta+theta0-thetaBmp-centerOff(k(i)+is),On(k(i)+is,:)/max(On(k(i)+is,:))
%     ...
    plot(theta+theta0-thetaBmp-centerOff(k(i)+is),Off(k(i)+is,:)/max(Off(k(i)+is,:
%     plot(dtheta+theta0,A(k(i),:)/max(A(k(i),:)),'-r')
%     plot(dtheta+theta0,A0/max(A0),':b')
%     text(27.24,.9,[num2str(newTime(k(i)),'%.1f') ' ...
    ns'],'FontSize',16)
%     xlabel('\theta (degrees)')
%     ylabel('Normalized Intensity')
```

```
294 %     xlim([27.239 27.255])
295 %     ax = gca; ax.FontSize=16;
296 %     title(num2str(centerShift(i)));
297 %     hold off;
298 %
299 %     figure(201);clf;
300 %     ...
    semilogy(theta+theta0-thetaBmp-centerOff(k(i)+is),On(k(i)+is,:)/max(On(k(i)+is
    on;
301 %     ...
    semilogy(theta+theta0-thetaBmp-centerOff(k(i)+is),Off(k(i)+is,:)/max(Off(k(i)+
302 %     semilogy(dtheta+theta0,A(k(i),:)/max(A(k(i),:)),'-r')
303 %     semilogy(dtheta+theta0,A0/max(A0),':b')
304 %     text(27.19,.5,[num2str(newTime(k(i)),'%.1f') ' ...
    ns'],'FontSize',16)
305 %     xlabel('\theta (degrees)')
306 %     ylabel('Normalized Intensity')
307 %     ax = gca; ax.FontSize=16;
308 %     title(num2str(centerShift(i)));
309 %     hold off;
310 %     i
311 %     jnk = input('Press Enter to Continue')
312 % end
313 %
```

REFERENCES

[1] Jean Baptiste Joseph Baron Fourier. *The analytical theory of heat*. The University Press, 1878.

[2] Timothy S Fisher. *Thermal energy at the nanoscale*, volume 3. World Scientific Publishing Company, 2013.

[3] David G Cahill, Paul V Braun, Gang Chen, David R Clarke, Shanhui Fan, Kenneth E Goodson, Pawel Keblinski, William P King, Gerald D Mahan, Arun Majumdar, et al. Nanoscale thermal transport. ii. 2003–2012. *Applied physics reviews*, 1(1):011305, 2014.

[4] Keith T Regner, Justin P Freedman, and Jonathan A Malen. Advances in studying phonon mean free path dependent contributions to thermal conductivity. *Nanoscale and Microscale Thermophysical Engineering*, 19(3):183–205, 2015.

[5] Li Shi, Chris Dames, Jennifer R Lukes, Pramod Reddy, John Duda, David G Cahill, Jaeho Lee, Amy Marconnet, Kenneth E Goodson, Je-Hyeong Bahk, et al. Evaluating broader impacts of nanoscale thermal transport research. *Nanoscale and Microscale Thermophysical Engineering*, 19(2):127–165, 2015.

[6] RB Wilson, Brent A Apgar, Lane W Martin, and David G Cahill. Thermoreflectance of metal transducers for optical pump-probe studies of thermal properties. *Optics express*, 20(27):28829–28838, 2012.

[7] Austin J Minnich, Jeremiah A Johnson, Aaron Jerome Schmidt, Keivan Esfarjani, Mildred Spiewak Dresselhaus, Keith A Nelson, and Gang Chen. Thermal conductivity spectroscopy technique to measure phonon mean free paths. *Physical review letters*, 107(9):095901, 2011.

[8] Keith T Regner, Daniel P Sellan, Zonghui Su, Cristina H Amon, Alan JH McGaughey, and Jonathan A Malen. Broadband phonon mean free path contributions to thermal conductivity measured using frequency domain thermoreflectance. *Nature communications*, 4(1):1–7, 2013.

[9] Ashok T Ramu and Yanbao Ma. An enhanced fourier law derivable from the boltzmann transport equation and a sample application in determining the mean-free path of nondiffusive phonon modes. *Journal of Applied Physics*, 116(9):093501, 2014.

[10] CW Li, Olle Hellman, Jie Ma, AF May, HB Cao, X Chen, AD Christianson, G Ehlers, DJ Singh, BC Sales, et al. Phonon self-energy and origin of anomalous neutron scattering spectra in snte and pbte thermoelectrics. *Physical review letters*, 112(17):175501, 2014.

[11] M Highland, BC Gundrum, Yee Kan Koh, Robert S Averback, David G Cahill, VC Elarde, JJ Coleman, DA Walko, and EC Landahl. Ballistic-phonon heat conduction at the nanoscale as revealed by time-resolved x-ray diffraction and time-domain thermoreflectance. *Physical Review B*, 76(7):075337, 2007.

[12] Yu-Miin Sheu, M Trigo, YJ Chien, C Uher, DA Arms, ER Peterson, DA Walko, EC Landahl, J Chen, S Ghimire, et al. Kapitza conductance of bi/sapphire interface studied by depth-and time-resolved x-ray diffraction. *Solid state communications*, 151(11):826–829, 2011.

[13] G Jackson Williams, Sooheyong Lee, Donald A Walko, Michael A Watson, Wonhuyk Jo, Dong Ryeol Lee, and Eric C Landahl. Direct measurements of multi-photon induced nonlinear lattice dynamics in semiconductors via time-resolved x-ray scattering. *Scientific reports*, 6(1):1–10, 2016.

[14] G Jackson Williams, Michael A Watson, Dohn A Arms, Timothy M Mooney, Donald A Walko, and Eric C Landahl. Epics oscilloscope for time-resolved data acquisition. *Nuclear Instruments and Methods in Physics Research Section A:*

Accelerators, Spectrometers, Detectors and Associated Equipment, 649(1):84–86, 2011.

[15] CR Wie, TA t Tombrello, and T Vreeland Jr. Dynamical x-ray diffraction from nonuniform crystalline films: Application to x-ray rocking curve analysis. *Journal of applied physics*, 59(11):3743–3746, 1986.

[16] Sergei G Podorov, G Hölzer, E Förster, and NN Faleev. Semidynamical solution of the inverse problem of x-ray bragg diffraction on multilayered crystals. *physica status solidi (a)*, 169(1):9–16, 1998.

[17] AA Stepanov. Fourier-coefficient method of x-ray rocking-curve interpretation. *Journal of applied crystallography*, 27(1):7–12, 1994.

[18] Sooheyong Lee, G Jackson Williams, Maria I Campana, Donald A Walko, and Eric C Landahl. Picosecond x-ray strain rosette reveals direct laser excitation of coherent transverse acoustic phonons. *Scientific reports*, 6(1):1–7, 2016.

[19] David W Hahn and M Necati Özisik. *Heat conduction*. John Wiley & Sons, 2012.

[20] Zlatan Aksamija. *Nanophononics: Thermal Generation, Transport, and Conversion at the Nanoscale*. CRC Press, 2017.

[21] Bertram Eugene Warren. *X-ray Diffraction*. Courier Corporation, 1990.

[22] Sergey A Stepanov. X-ray server: an online resource for simulations of x-ray diffraction and scattering. In *Advances in Computational Methods for X-Ray and Neutron Optics*, volume 5536, pages 16–26. International Society for Optics and Photonics, 2004.

[23] Sergey A Stepanov. X-ray server, 2004. Available at https://x-server.gmca.aps.anl.gov.

[24] Eric C Landahl. Time-resolved x-ray diffraction, 2008. Available at https://github.com/elandahl/dynamical-diffraction.

[25] John D'Errico. Slm - shape language modeling, 2017. Available at https://www.mathworks.com/matlabcentral/fileexchange/24443-slm-shape-language-modeling.